5-2013

Supersonic Turbine Cascade Studies Using Computational Fluid Dynamics and Water Table Experiments

Shelby E. Nelson
University of Nevada, Las Vegas, shelby.e.nelson@gmail.com

SUPERSONIC TURBINE CASCADE STUDIES USING COMPUTATIONAL FLUID DYNAMICS AND WATER TABLE EXPERIMENTS

by

Shelby E Nelson

Honors Thesis submitted in partial fulfillment
of the designation of Department Honors
Mechanical Engineering
Dr. Yitung Chen, Advisor
Dr. Bill Culbreth, Committee Member
Dr. Andrew Hanson, Committee Member
College of Engineering
University of Nevada, Las Vegas
May, 2013

ABSTRACT

Design engineers use a variety of tools to perform calculations and to aid in the design process. For example, engineers designing gas turbines, specifically the aerodynamicists, use a combination of hand calculations, experimental data, and complex numerical codes to simulate air flow around each blade. Aerodynamicists designing gas turbines must predict the locations of the shocks to locate inefficiencies in the flow. In this thesis, three methods of calculating the shock angles are compared: analytical, experimental, and computational. Three different airfoil shapes are tested: a rectangular flat plate, a supersonic diamond, and a turbine airfoil. Cascade tests of the airfoil shapes were also performed. Hand calculations using the compressible flow theory with shock analysis are performed on simplified single airfoil cases. The experimental rig used is a water table apparatus that simulates compressible flow. The different airfoils and configurations were tested in the water table and photographs were taken. ANSYS Fluent, a commercial Computational Fluid Dynamics (CFD) code, is run on each case. Due to the complex nature of the flow, hand calculations, experimental data, and CFD results are only compared for the flat plate and supersonic diamond single airfoil cases. The results from each method are compared and the percent error is taken to determine the accuracy of each method. All three methods produced results that were in an acceptable range of error for the flat plate. The analytical and computational for the supersonic diamond cases matched up within acceptable error, but the experimental results were off by a maximum of about 40%.

INTRODUCTION

Gas turbines are used for a variety of purposes. They are used in industrial applications to generate power as well as in aviation as jet engines to provide thrust to propel an aircraft in flight. A gas turbine is an axial flow turbomachine consisting of a compressor, combustor, and a turbine. The compressor sucks in air from the atmosphere and compresses it through multiple stages. General Electric's 7FA turbine engine uses a 14 stage compressor. The air enters the compressor and is compressed. The compressed air enters a combustion chamber where it is injected with fuel and ignited. The hot air is then accelerated through a turbine which extracts the usable energy from the flow as it rotates. The flow then rushes through the exhaust nozzle and propels the aircraft forward. Figure 1 shows a transparent model of an industrial gas turbine (Martin, Forry, Maier, & Hans, 2012). The different components are easily seen.

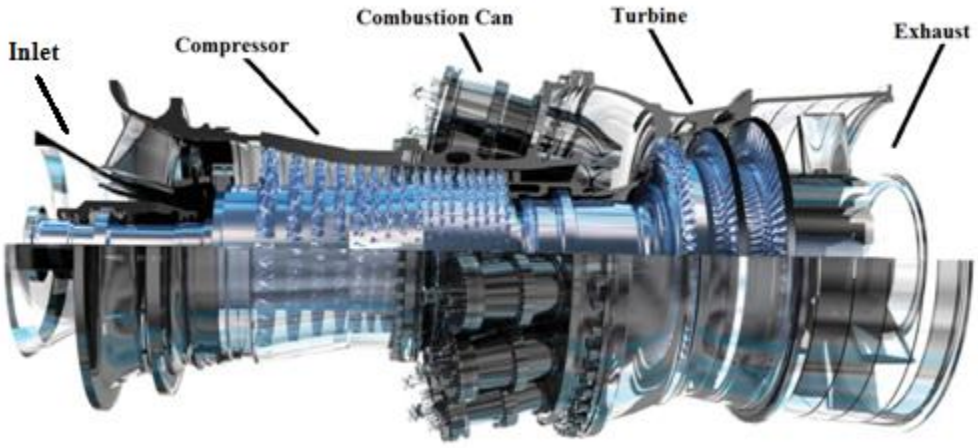

Figure 1 - General Electric's 7FA Engine (Martin, Forry, Maier & Hans, 2012)

The velocity of the air in the turbine often times exceeds the speed of sound, or Mach 1. When the flow is above Mach 1, shocks form. Predicting the location of shocks in supersonic flow is important because shocks are major disruptions in the flow which restrict the flow making the gas turbine less efficient.

The purpose of this thesis was to analyze the shock location in a supersonic turbine cascade by comparing the results of the analytical, experimental, and numerical solutions. It is important to validate these three methods because they are used by engineers to design gas turbines that will generate power in power plants or provide vital thrust on a jet airplane. A supersonic turbine cascade experiences flows above Mach 1. Supersonic flow is studied because there are advantages to increasing the velocity and temperature of the flow to achieve higher performance in gas turbines. This project analyzed the shock angles produced from different airfoil geometries in various cascade configurations in two-dimensional supersonic flow.

This thesis was divided into three separate approaches to finding the shock angles: 1) analytical, 2) experimental, and 3) computational. The results from each section were compared using the analytical as a control. The analytical serves as the theoretical baseline. Background information on the three methods for analyzing shock angles is described below.

Analytical Approach

Hand calculations were performed using the compressible flow theory to solve for shocks around the airfoil. In compressible flow, the density of the fluid is not uniform. This means that the molecules of the fluid are able to compact very close together in some areas and not necessarily have the same compactness in other areas. There are regions in the fluid where the density is different than other regions. For this reason, shocks, or discontinuities in the flow, occur where the flow is accelerated very quickly.

Shock waves are areas in the flow where the static pressure and temperature increase instantaneously. Shock waves occur in fluid moving faster than M=1. At speeds this fast, the flow does not have time to adjust for objects in its path. The object in the flow path causes a

disturbance within the flow. In supersonic flow, the molecules around the object do not have enough time to collide with each other and communicate with molecules upstream that there is an object in the way. The flow is moving too fast for molecular disturbances to level out, so the molecules begin to pile up and the fluid compresses forming a shock wave around the object (Anderson, 2007).

Three different types of compressible flow phenomena occur in flow over airfoils: normal shocks, oblique shocks, and expansion fans. Normal shocks occur perpendicular (90°) to the upstream flow. They generally form as bow waves in front of blunt objects. An oblique shock forms an oblique (less than 90°) angle. They form where the flow is suddenly directed around a concave corner. The total pressure increases discontinuously across a shock wave causing a buildup of pressure where the shock occurs (Anderson, 2007). Expansion fans are also discontinuities in the flow where pressure decreases rapidly. Expansion fans generally occur at an oblique angle to the flow and form around convex corners, or away from the flow (Anderson, 2007). Figure 2 shows a diagram of an oblique shock and expansion fan.

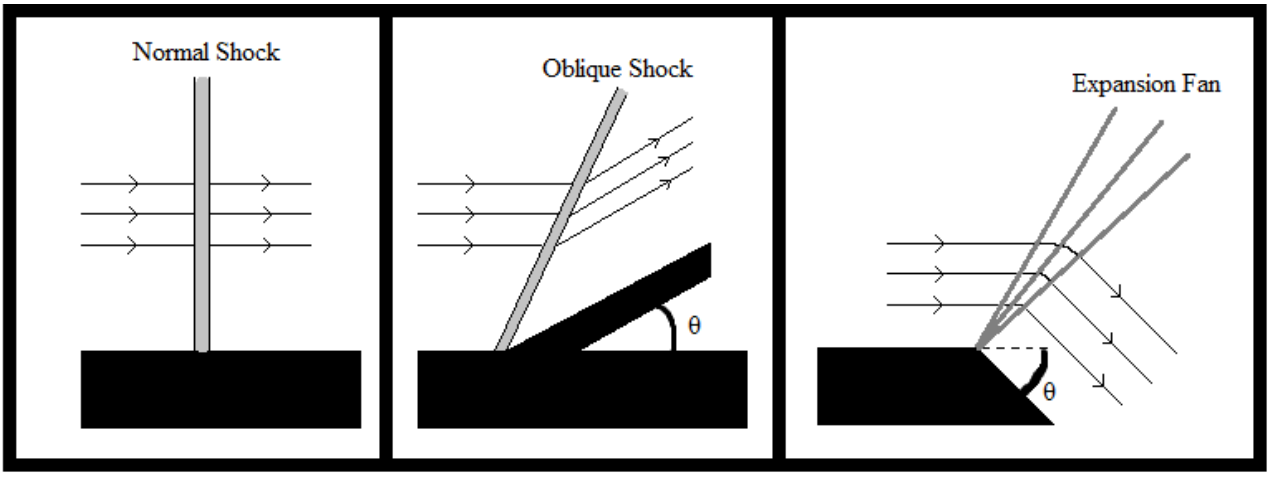

Figure 2 –Normal Shock, Oblique Shock, Expansion Fan. The black lines and arrows represent the fluid flow direction, and the angle, θ, represents the deflection angle of the surface. (Anderson, 2007)

Experimental Approach

Compressible flow is highly dependent upon the Mach number of the flow, defined as the ratio of the flow velocity to the speed of sound. There is a strong analogy between shocks and shock angles in compressible flow and hydraulic jumps in surface flows in water. Hydraulic jumps are apparent as abrupt changes in water depth, such as bow waves formed from objects moving through water. The angle of hydraulic jumps is a strong function of Froude number, defined as the ratio of flow velocity to gravitational velocity, $Fr = V/\sqrt{gy}$. This analogy allows us to use water tables to generate hydraulic jumps around objects. The bow waves formed at a specific Froude number has the same angle as a bow shock formed when M = Fr.

A water table was used to test the different airfoil geometries and configurations in a water fluid domain that simulates compressible flow in air. The water table, shown in Figure 3, is a subsonic test apparatus that is used for testing how fluid (water) reacts to different geometric shapes when they are placed within a flow region.

Figure 3 – UNLV Water Table Apparatus

The water table is a subsonic alternative to testing supersonic airflow in an expensive pressurized wind tunnel. If the hydraulic jump analogy to compressible flow is assumed, the water table provides an accurate visual representation of shock locations.

Hydraulic jump is a phenomenon that occurs in open channel flow when fluid of high velocity and low velocity meet. These fluids are moving at a subsonic rate. Since the mass flow rate and momentum are the same in the fluid, the high velocity fluid must slow down abruptly to match the low velocity fluid. To compensate, the high velocity fluid will convert some of its kinetic energy to potential energy seen as a change in height of the fluid. Figure 4 shows a picture of hydraulic jump from a faucet (Bush & Aristoff, 2008). The high velocity of the water coming out of the faucet hits the bottom of the sink and spreads. The water that gets farther away from the faucet slows down creating a region of fluid with low velocity. The height difference is clearly seen where the fluid of high velocity from the faucet meets the region of low velocity. This height difference can be measured and the Froude number, a dimensionless quantity describing the flow, can be calculated.

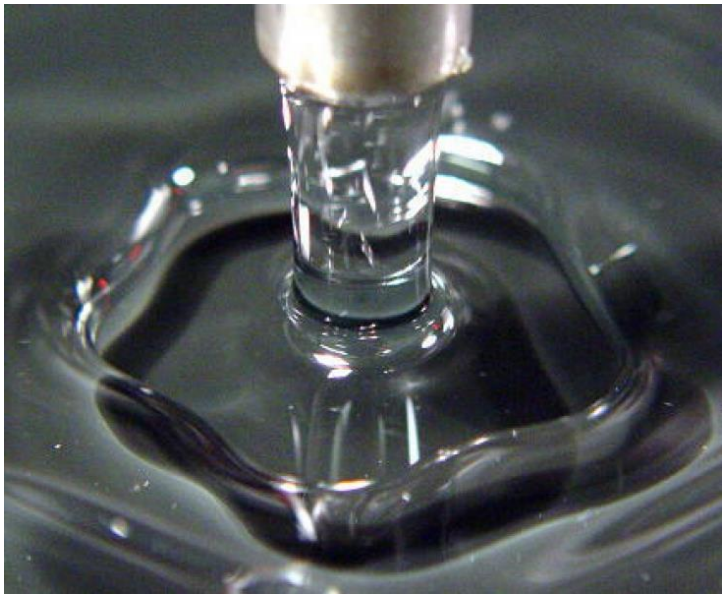

Figure 4 - Hydraulic Jump Forming Around a Faucet (Bush & Aristoff, 2008)

Computational Approach

Since the flow inside a gas turbine is very complex to solve by hand, engineers use a numerical simulation to predict the flow. CFD is used to predict the locations of the shocks. The Navier-Stokes equations that govern flow in a continuum are the basis for CFD solvers. Since the equations contain multiple unknowns, non-linear terms, and second-order partial differential equations for complicated flow problems, hand calculations are impossible (Pritchard, 2011). CFD uses numerical methods to simultaneously solve for the unknowns and complicated terms for each element in the mesh.

The commercial software used in this numerical calculation is ANSYS Fluent. This solver uses the finite volume method to solve the flow properties in a finite volume around each node in the mesh. An iterative solver was used to solve each cell in the grid in this study. The solver continues to iterate until the error of each variable in the governing equations has reached the selected convergence value.

In this study, the shock angles about several airfoil shapes will be compared using results from analytical calculations using compressible flow theory and from the computational fluid dynamics package, FLUENT. The results will also be compared to photographs obtained from a water table that exploits that analogy between compressible flow and hydraulic jumps when the Froude numbers and Mach numbers are matched.

LITERATURE REVIEW

(1)

For the different approaches to find the shock angles in this thesis (analytical, experimental, and computational), important guidelines found in past research were used.

Analytical Approach

In order to use the compressible flow theory, certain assumptions about the fluid flow were made. The flow is assumed to be steady. The Reynolds number, a ratio of inertial forces to viscous forces, was calculated to be 4.09 x 10^6 which is considered to be infinite. This means that the inertial forces outweigh the viscous forces in the fluid. Because of this, the flow is assumed to be an inviscid (dynamic viscosity should approach to 0). The flow is considered adiabatic with no body forces, such as gravity. The fluid, being air, is considered an ideal gas, or calorically perfect (Anderson, 2007). Also, the flat plate was assumed to be infinitely thin.

Experimental Approach

The Froude number is a dimensionless quantity. It is a ratio of the fluid velocity to the gravitational wave velocity. It is calculated by measuring the bow wave from an object and plugging it into Equation (1) It can also be calculated by measuring the height of the fluid before the jump and after the jump and plugging them into Equation (2).

$$Fr = \frac{1}{\sin(\theta)} \qquad (1)$$

$$\frac{h_2}{h_1} = \frac{\left(\sqrt{1+8Fr^2}-1\right)}{2} \qquad (2)$$

In the hydraulic jump analogy, the Froude number is analogous to the Mach number in compressible flow (Fr = M), so a bow wave in the water table will have the same wave angle as a shock in compressible flow (Culbreth, 2012). The locations of the hydraulic jumps that occur

around each of the airfoil geometries in the water table are where the shocks are predicted to form in supersonic compressible flow. The hydraulic jump will be seen in distinct lines coming from the airfoil geometry. The angle of these lines is measurable and can be compared with the angles from the analytical calculations.

A water table apparatus is a useful apparatus to test two-dimensional flow problems. The diagram below in Figure 5 shows the main components of the water table. The reservoir is filled to the desired level with water from a hose. The pump is turned on and the flow gate is opened. The flow of the water through the pump is controlled by a turn knob. Water is flooded over the test section and spills into the spill tank. The water circulates back through the pump and into the reservoir to provide a continuous flow over the test section. The test section of the water table allows for a good visual representation of the reaction of the flow across a two-dimensional cross-section of an airfoil. Since a cross-section of an airfoil is used, the flow across the whole wing is assumed to be the same at each span.

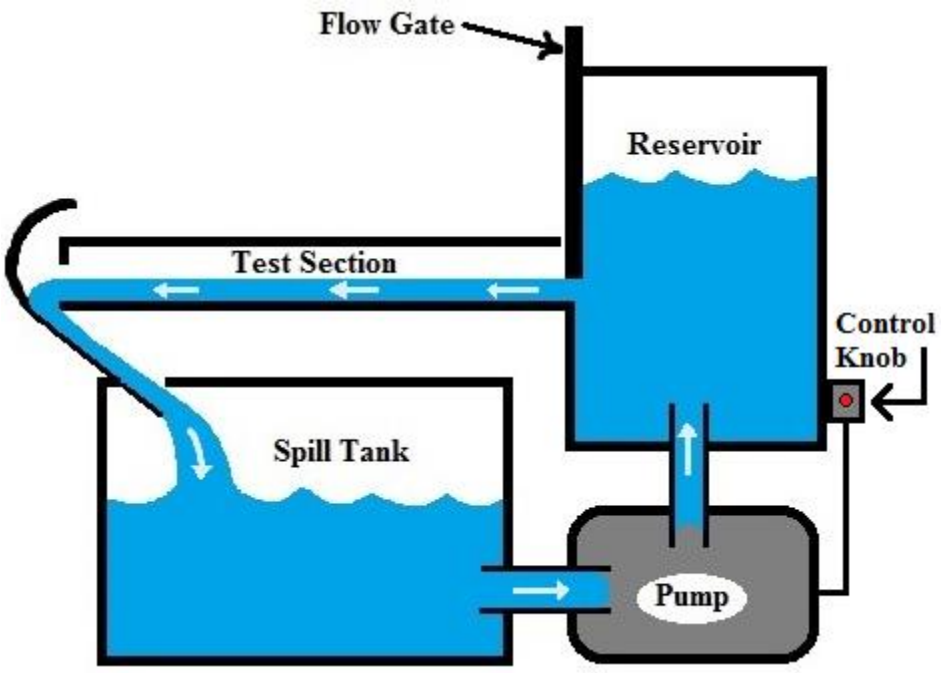

Figure 5 - Water Table Basic Components (not to scale)

Computational Approach

Creating the geometry of the airfoil and the fluid domain is the first step in setting up the CFD simulation. Standard practices dictate the dimensions of the fluid domain should be two times the chord length before the airfoil and five times the chord length after the airfoil with a width of ten times the airfoil chord length. A diagram is shown below in Figure 6 for a better visual representation.

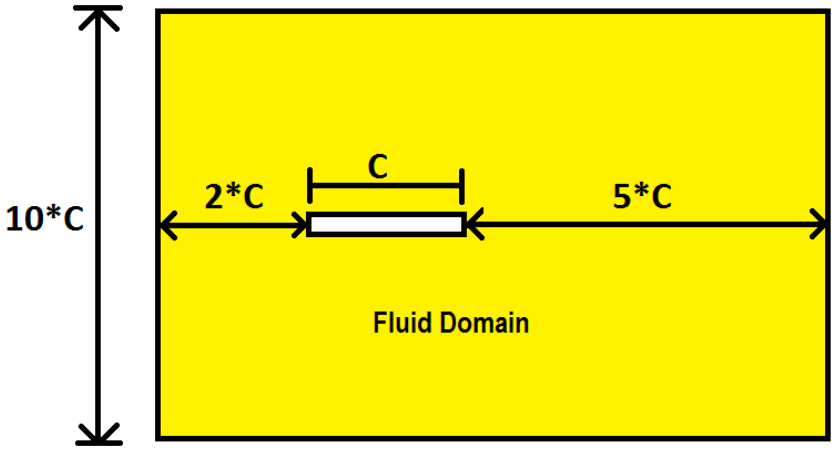

Figure 6 – Fluid Domain Standard Dimensions (not to scale)

Meshing the fluid domain is the next step in solving CFD problems. In this thesis, a structured mesh was used. The flow field was first meshed with a finite number of elements. The number and size of these elements are important considerations in mesh quality. The number of elements should be fine enough to capture important geometry, but not too fine as to crash the memory of the computer (Tu, Yeoh & Liu, 2008). Another important mesh factor to consider is the aspect ratio of the cells. Aspect ratio is the height of the cell divided by the width. An aspect ratio between 0.2 and 5 is acceptable (Tu, Yeoh & Liu, 2008). If the aspect ratio is too large or too small, the solution will be inaccurate and the job will have a difficult time in converging. Another mesh guideline is the skewedness (orthogonal quality) of the elements. For example, a perfect square will have a skewedness angle of 90°. Anything less than or greater than that angle

distorts the square into a parallelogram. Typical allowable skewedness angles range from 45° to 135° (Tu, Yeoh & Liu, 2008). Figure 7 is an example of a good structured mesh that meets all the above criteria (Gallardo, 2010).

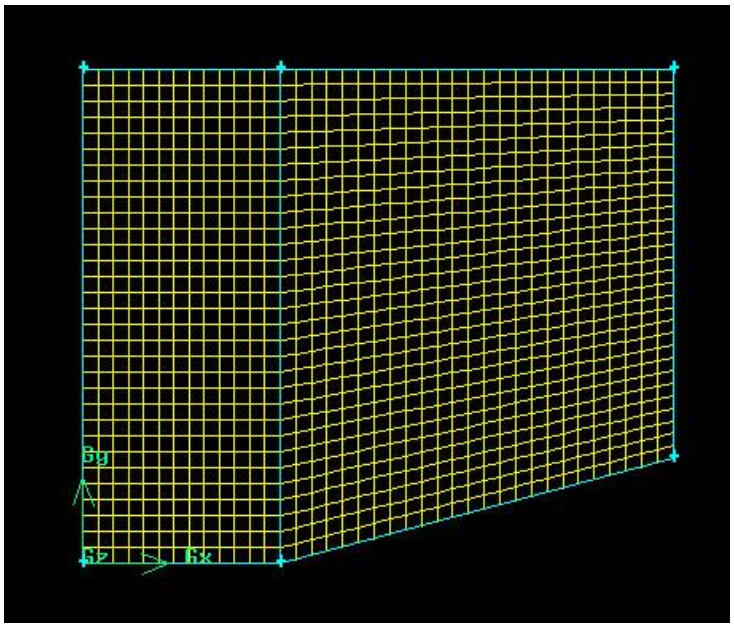

Figure 7 – Example of a Good Mesh (Gallardo, 2010)

Setting up the flow conditions and solution criteria is the final step before the simulation is run. For complicated programs such as ANSYS Fluent, it helps to have a reference off of which to base future cases. An example of a supersonic flow over a wedge was found on an internet Fluent tutorial that has similar flow conditions to the cases in this thesis (Gallardo, 2010). The flow physics and solution criteria in this thesis were modeled after this example. The same density-based solver was used to model compressible flow. The rest of the flow properties used from this example can be found in Appendix A.

METHODOLOGY

Geometry Selection

The different airfoil geometries for this thesis were chosen to provide a broad understanding of how shocks form around different shapes. The geometries that were analyzed are listed below:

1) Flat Plate
2) Supersonic Diamond
3) Turbine Blade

The dimensions of the different airfoils are seen in the CAD drawings in Figure 8. These dimensions were chosen because they best fit in the test section of the water table.

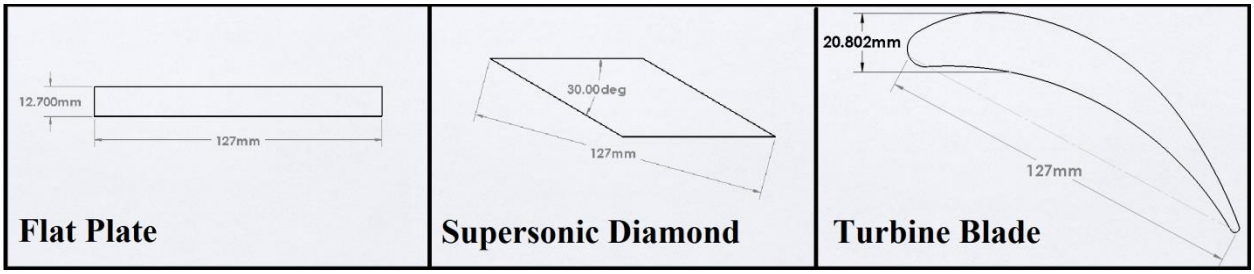

Figure 8 – CAD (SolidWorks) drawings of the three airfoil geometries used in this project (not to scale)

This project will examine the flow around the following configurations of the geometries listed above. The diagram in Figure 9 shows the configurations for the cases analyzed in this project. The cases are numbered in Table 1 below.

Table 1 - Cases Considered

Case #	Configuration	Geometry	AOA (°)
1	Single Airfoil	Flat Plate	0
2	Single Airfoil	Flat Plate	4
3	Single Airfoil	Supersonic Diamond	0
4	Single Airfoil	Supersonic Diamond	4
5	Cascade	Flat Plate	0
4	Cascade	Flat Plate	4
6	Cascade	Supersonic Diamond	0
8	Cascade	Supersonic Diamond	4
9	Single Airfoil	Turbine Blade	0
10	Cascade	Turbine Blade	0

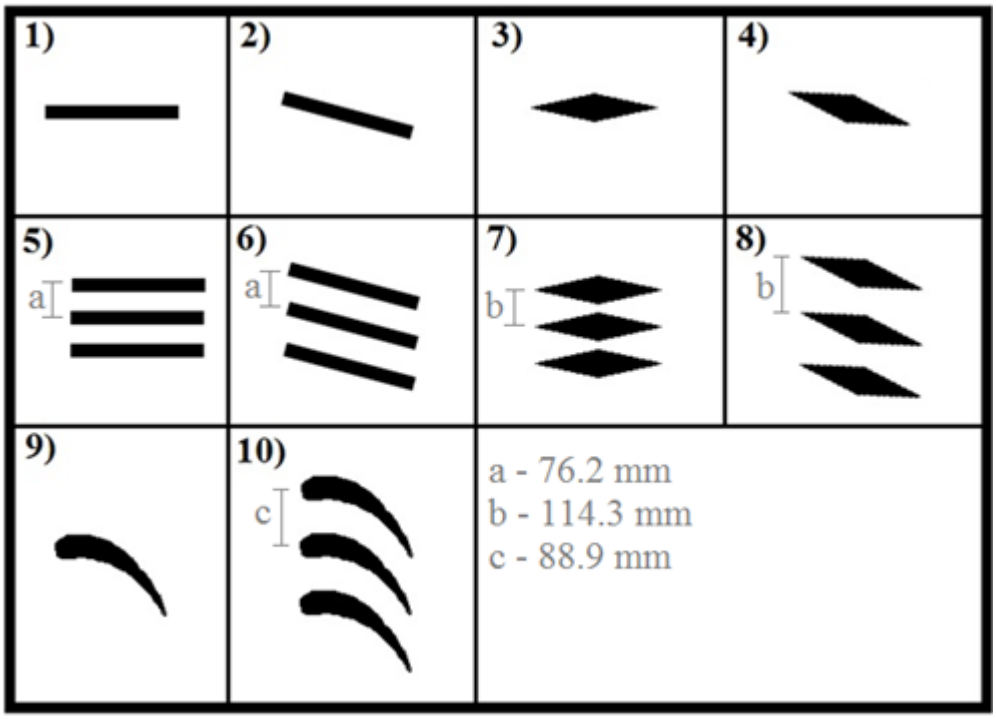

Figure 9 – Configurations Studied (not to scale): The flow moves from left to right. The numbers correspond to the case numbers in Table YY1a.

Water Table Set-Up Procedure

The water table must be plugged in to an electrical outlet to run the pump. A hose was placed in the reservoir and is turned on. The water will flood into the pump and will start filling up the spill tank. Once the water in the spill tank has reached the height of the reservoir (water

will start accumulating in the reservoir), the hose is turned off and taken out of the reservoir. The water table is now ready to operate.

Froude Number/Mach Number Calculation

The water table was used to find the Mach number from the Froude number. This Mach number was used in the hand calculations, experiment, and CFD.

The water table was turned on. The flow gate was adjusted to an approximated 3 mm opening. The flow was adjusted by the control knob, so the water flowing across the test section will yield a Froude number of about 1.5. Since there was no way of determining what flow rate the pump was producing, the experimenter must "guess and check" by turning the knob and calculating the Froude number.

The Froude number was calculated in two ways. The first method of calculating the Froude number was by measuring the angle of the bow shock. A flat plate was placed parallel to the flow (shown in Figure 10). The plate was adjusted so that the angles of the hydraulic jumps ($\theta 1$ and $\theta 2$) are symmetric. The hydraulic jump angles were measured, and the average was taken. Table 2 shows the two measured values and its average.

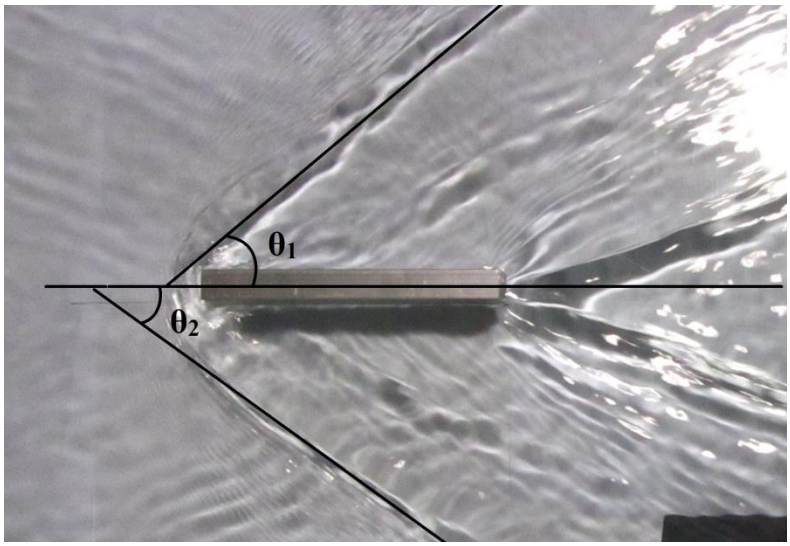

Figure 10 - Bow Shock Method for Calculating Hydraulic Jump: θ1 and θ2 are the angles of the hydraulic jump. Because of flow symmetry, θ1 ≈ θ2.

Table 2 - Measured Values of Hydraulic Jump Angle

θ_1	41°
θ_2	40°
$\boldsymbol{\theta_{Average}}$	40.5°

The Froude number was found from the following equation. Using the average value of θ, the measured Froude number was calculated. The equation to calculate the Froude number is found below.

$$Fr = \sin^{-1}\left(\frac{1}{\theta}\right)$$

$$Fr = 1.54$$

The second method uses the height difference in the fluid and is called the conjugate depth method. A flat plate was placed perpendicular to the flow shown in the photograph in Figure 11. The plate was placed perpendicular to the flow so that a large bow wave was formed where the water jumps, and the measurements were easily taken. The heights are measured with a caliper at three different points before and after the hydraulic jump.

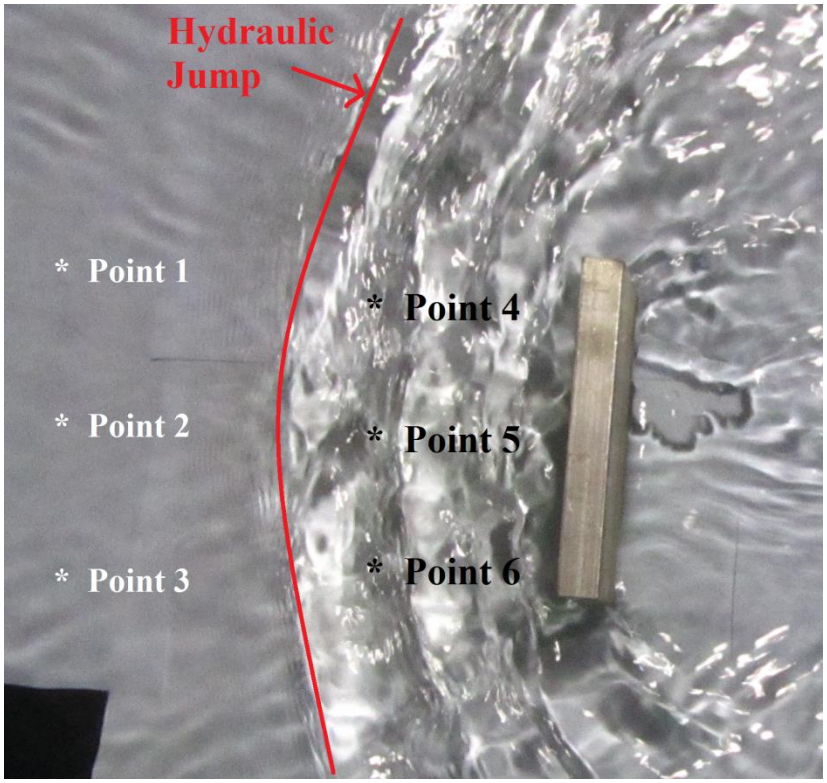

Figure 11 – Airfoil Set-Up for the Conjugate Depth Method: The fluid is moving from left to right. The red line shows the location of the hydraulic jump bow wave. Points 1-3 (white) are measured for the value of h1, and Points 4-6 (black) are measured for the value of h2.

The points were averaged to get a single value of h_1 and h_2. Table 3 shows the measured values and their averages.

Table 3 - Measured Values for the Conjugate Depth Method. The measured depth before the jump is h1, and the measured depth after the jump is h2.

	h1 (mm)		**h2 (mm)**	
	Point 1	10.14	*Point 4*	18.72
	Point 2	10.52	*Point 5*	17.84
	Point 3	9.99	*Point 6*	18.49
Average	**10.21**		**18.35**	

The Froude number was calculated using the average values of the two depths. The depths were plugged into the equation below.

$$\frac{h_2}{h_1} = \frac{\sqrt{1 + 8Fr^2} - 1}{2}$$

$$Fr = 1.585$$

The two values of the Froude number found in the conjugate depth method and the bow shock method are averaged to get a final Froude number of

$$Fr = 1.56$$

This Froude number was used for all the experiments performed on the water table. Because of the hydraulic jump analogy to compressible flow, the value of the Froude number equals the value of Mach number.

$$M = 1.56$$

This Mach number was used as the inlet Mach number for the analytical hand calculations and in the CFD simulations.

Analytical Method

An airfoil is a complicated shape, so a simplified model is chosen to predict the location of shocks. As the case number increases, the more complex the geometry, and hand calculations become more difficult. Because of time constraints and increased complexity of each case, hand calculations were only performed on Cases 1-4.

The incoming flow conditions were the same for all cases. M1 and P1 were the incoming Mach number and pressure respectively. These values are given below and are the same for all cases. In Figures 12-15, the incoming flow is horizontal and is represented by the arrow. The Mach number calculated from the Froude number is found below.

$$M_1 = 1.56$$

Case 1-Flat Plate, Single Airfoil, at 0° AOA

Case 1 is shown in Figure 12 below. The incoming flow is represented by the arrow. The Mach number is given below. The lines coming from the flat plate are the anticipated shock lines. The shock lines divide the flow up into two regions. Since the flat plate has a 0° angle of attack, the flow is symmetric, so the region underneath region 2 will have the same properties. The following calculation assumes that the flat plate is infinitely thin for simplicity.

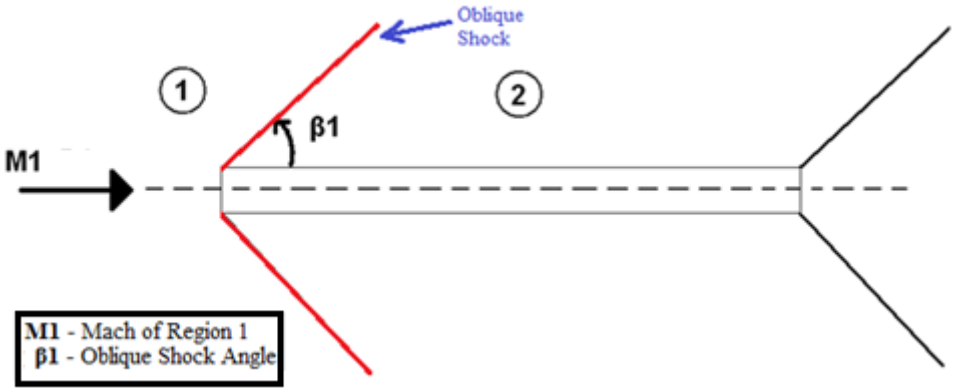

Figure 12-Flat Plate at 0° Angle of Attack (not to scale): The red line represents the predicted location of the oblique shock.

The shock angle, β_1, was found from the Theta-Beta-Mach diagram, a standard diagram found in Appendix C. The Theta-Beta-Mach diagram gives the relation of the deflection angle, theta, the shock angle, beta, and the Mach number. Since the incoming flow is at a 0° angle of attack and the surface of the plate is parallel to the incoming flow, the deflection angle is 0°.

Case 2- Flat Plate, Single Airfoil, at 4° AOA

The diagram for this case is shown in Figure 13. The flow was divided into three separate regions.

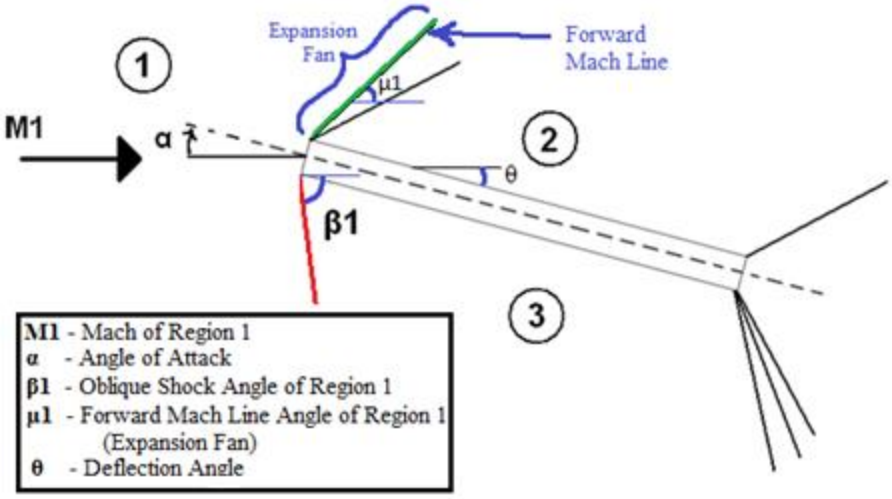

Figure 13-Flat Plate at 4° AOA (not to scale): The red line represents the predicted location of the oblique shock. The expansion fan is represented by the green and black line above the oblique shock. The green line in the expansion fan is the forward Mach line.

Region 1 to 3, where the oblique shock is located, was analyzed. The deflection angle, θ, is the same as the AOA, α, since the flat surface of the plate is angled down at a 4° angle. Since the incoming Mach number (M=1.56) and the deflection angle (θ=4°) are known, the Theta-Beta-Mach diagram (Anderson, 2007) was used to find the angle of the oblique shock, β1.

Next, Region 1-2 was analyzed. Using the incoming Mach number, the angle of the forward Mach line of the expansion fan was calculated with the following equation.

$$\mu_1 = \sin^{-1}\left(\frac{1}{M_1}\right) \qquad (3)$$

Case 3 – Supersonic Diamond, Single Airfoil, at 0° AOA

Figure 14 is a diagram of Case 3. Since the flow is symmetric, the flow can divided into four regions. Region 4 is neglected because it has no effect on the airfoil. However, the bow shock separating Region 1 and 4 was the only shock phenomenon that was analyzed for this case. This is because the angles expansion fans (Region 2 to 3) were not able to be measured in

the experiment or the CFD; however, the angles can be calculated by knowing the Mach number of Region 2 and using Equation (3) to find the angle of the forward Mach line.

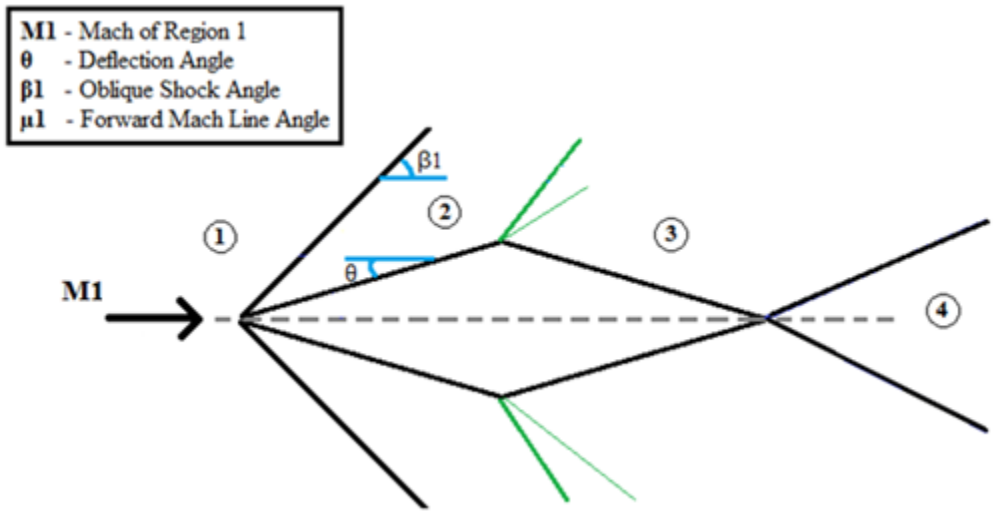

Figure 14- Supersonic Diamond, Single Airfoil, at 0° AOA: Shocks are represented by the black lines. The Expansion fan is represented by the green line. The deflection angle, θ, is equal to 15°.

It was discovered that the deflection angle, $\theta = 15°$, is greater than the maximum allowable angle, so the shock for this case is detached. Since detached shock calculations are fairly complex to do by hand, the Mach number was increased to 2.2. Increasing the Mach number allows for a larger deflection angle.

After the Mach number was increased to M=2.2, the same principles that were used to solve Cases 1 and 2 were implemented in analyzing this case. The values that were obtained are found in Table 5 in the Results section.

Case 4 – Supersonic Diamond, Single Airfoil, at 4° AOA

Figure 15 shows a diagram of Case 4. Since the flow is not symmetric around the airfoil, it is divided up into six regions. Region 4 is neglected since it has no effect on the airfoil.

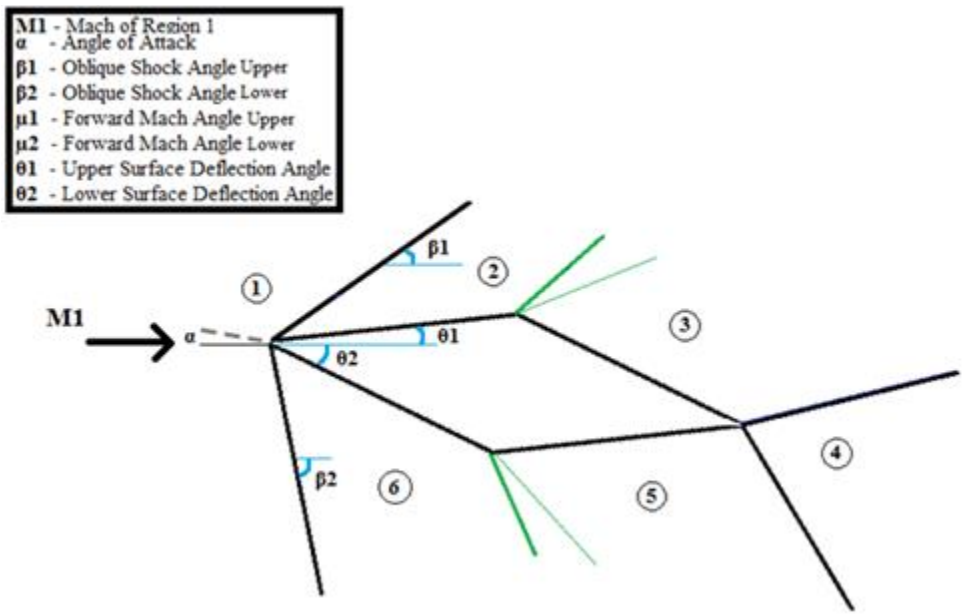

Figure 15 - Supersonic Diamond, Single Airfoil, at 4° AOA: The black lines represent the shocks, and the green lines represent the expansion fan. With an angle of attack of 4°, the upper deflection angle, θ1, is equal to 11°, and the lower deflection angle, θ2, is equal to 19°.

The Mach number for this case was also increased to M=2.2 to get rid of the detached shock. The following values were found by using the same shock and expansion fan principles used in Cases 1-3. The values that were obtained are found in the Results section.

Airfoil Construction

The airfoils were constructed in the UNLV Engineering machine shop with available shop materials. Table 4 below lists the material used and the machining method to create each part. Aluminum was chosen because it is easy to machine, and it is heavy enough to not float away when put in the water table.

Table 4 - Material/Machining Method of Airfoil Shapes

Airfoil Shape	**Material**	**Machining Method**
Flat Plate	0.5 in x 1.0 in Aluminum Rectangle Stock	Vertical Band Saw
Supersonic Diamond	0.75 in Aluminum Plate	Vertical Band Saw
Turbine Blade	0.75 in Aluminum Plate	CNC Mill

Figure 16 shows the final machined airfoil geometries to be tested in the water table.

Figure 16 – Aluminum Airfoil Geometries to Be Tested in the Water Table

Experimental Method

To experimentally test the compressible flow theory without a supersonic wind tunnel, a water table was used assuming the hydraulic jump analogy. The dimensions of the water table are shown in the photograph in Figure 17.

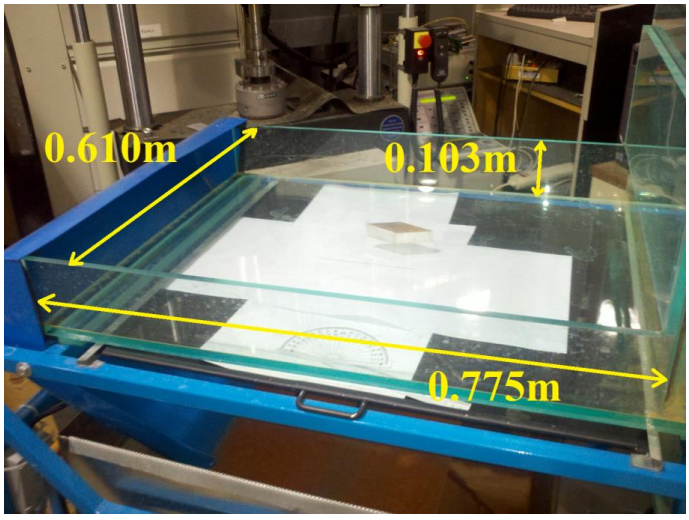

Figure 17 – Dimensions of the test section of the water table

The flow of the water table was adjusted to a Froude number of 1.56 (calculated above). The flow of the water was adjusted by a knob on the control box, but there was no display showing at what flow rate the water is flowing. The user must do trial and error to arrive at the correct Froude number by the conjugate depths method or the bow shock method.

Cases 1-10 were tested in the water table. The airfoils were placed in the center of the water table, so that the effects of the hydraulic jumps interacting with the boundaries of the test section are minimized. Photographs were taken with a digital camera 2 to 3 feet directly above the test specimens. The angle of attack of the airfoils was measured by a protractor placed under the clear bottom. The airfoils were placed at a 0° and 4° angle of attack to match the configurations shown in Figure 3. The photographs are found in the Results section.

After realizing that the shock was detached for Cases 3 and 4 for a Froude number of 1.56, the water table experiment was repeated at a Froude number of 2.2.

Computational Procedure

ANSYS Fluent was the CFD software that was used to predict the shock locations for Cases 1-10. ANSYS Fluent has different steps to go through when a project is first created. The steps are listed below. A more detailed procedure is found in Appendix A.

1) Geometry: The geometry of the airfoil and the fluid domain were created in the ANSYS geometry editor.

2) Mesh: The mesh is created using the settings found in Appendix A. The mesh is refined around the airfoil to properly capture the boundary layer. The meshes for Case 1, 5, and 9 can be found in Figures 18-20 below.

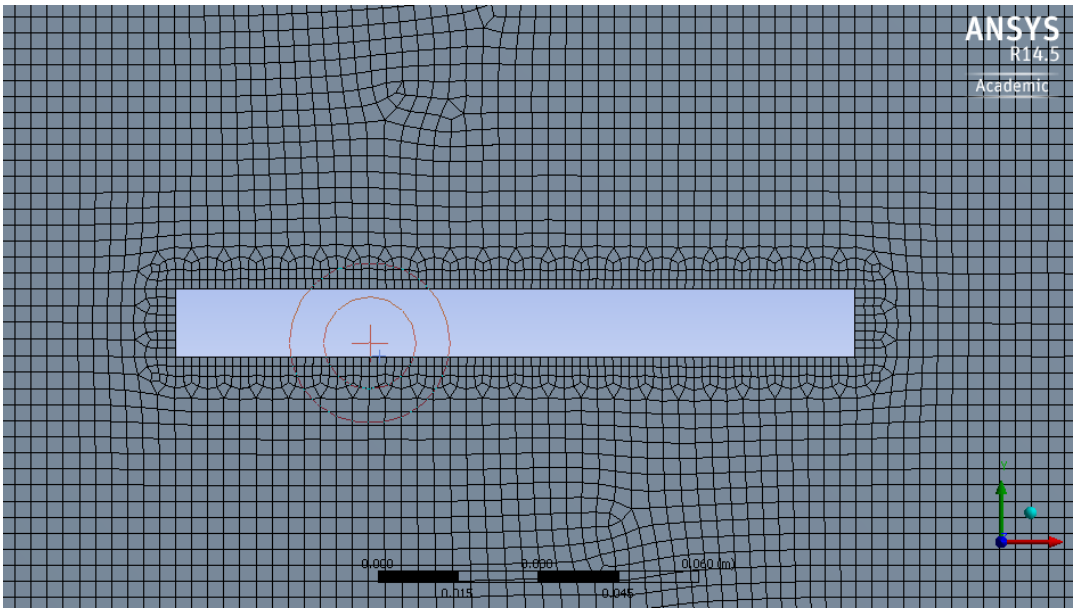

Figure 18 – Case 1: Flat Plate Mesh

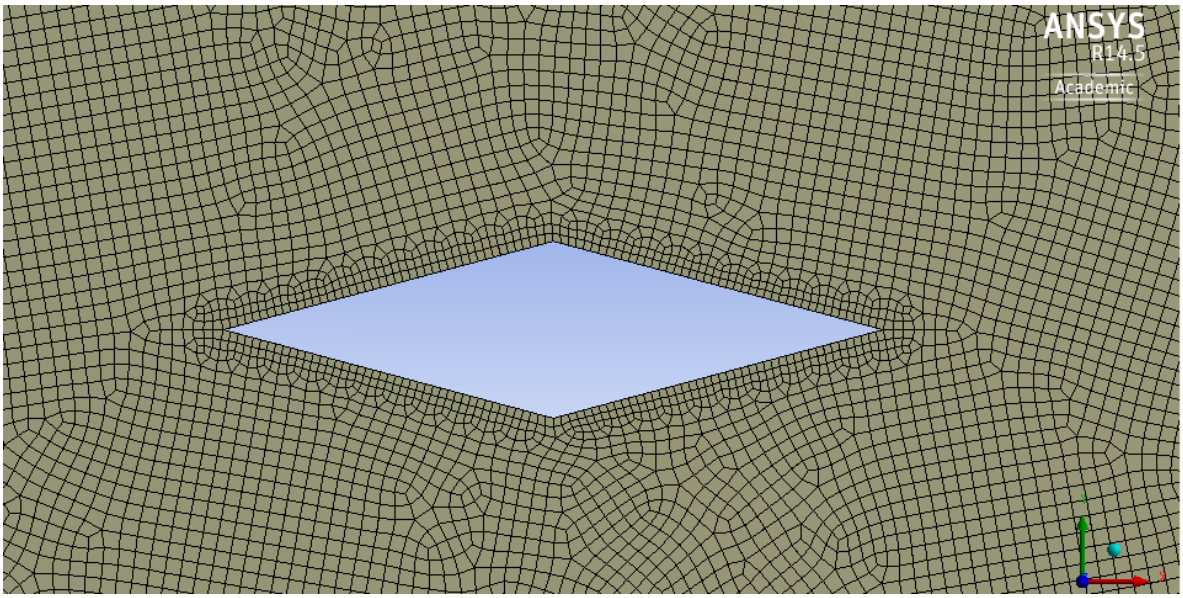

Figure 19 – Case 3: Supersonic Diamond Mesh

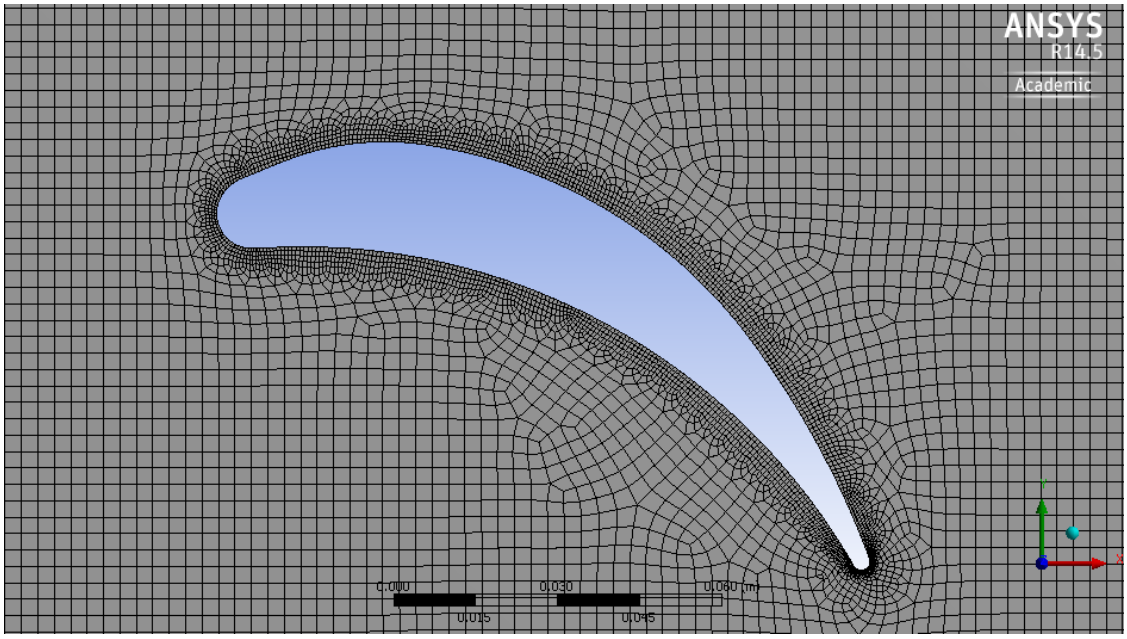

Figure 20 – Case 9: Turbine Blade Mesh

3) Set-Up: In this section, the physics of the problem are specified. This includes the boundary and flow conditions. The details of the set-up can be found in Appendix A.
4) Solution: This section is where the details of the solver are specified. The solution is initialized, and additional solving parameters are specified.

After realizing that the shock was detached for Cases 3 and 4 for a Mach number of 1.56, the CFD was repeated at a Mach number of 2.2 for these cases.

RESULTS

The results of the experimental and CFD are shown below in Figures 21-30. The photograph of the experiment in the water table is shown on the left (a), and a contour plot of the static pressure is shown on the right (b).

The bow shock angles of the analytical results were calculated using the compressible flow theory. These results are found in Table 5.This project refers to the shock or expansion fan that is created at the beginning of the airfoil as “bow shock.”

The angles of the bow shock were measured from the photograph of the experiment. Lines were drawn on the hydraulic jump line shown in Figure 21 (a). For the flat plate, the bow shock cannot be drawn as a straight line from the tip of the leading edge away from the airfoil. This is because there is a strong normal shock on the front surface of the leading edge. The angle of a normal shock is 90°, so the shock needs to have enough space to curve around the flat plate. A line was drawn from the outermost region of the shock to the centerline of the flat plate. After the lines were drawn, the photographs were printed out, and the angle was physically measured with respect to the incoming flow with a protractor.

The angles of the computational results were found by selecting two points in Fluent that were located on the shock. Since the shock is a rapid increase in pressure, the location of the shock is easily seen on the contour plot of static pressure. By finding the vertical and horizontal distance between the two points and doing an arctangent relation, the angle of the shock was found.

The angles found from the three methods were compared, and the percent error was calculated. The percent error is found in Table 6.

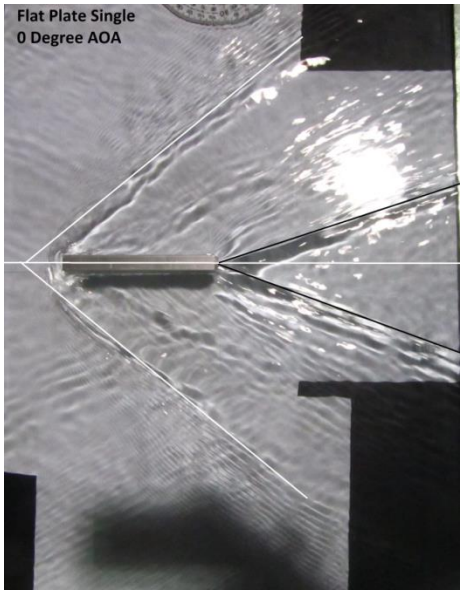

(a) Water table photograph: Lines were drawn to show shock locations with respect to the horizontal incoming flow.

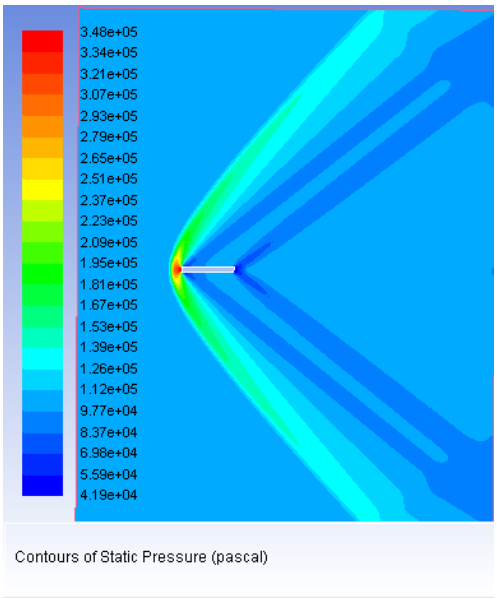

(b) CFD result showing static pressure

Figure 21 – Case 3: Flat plate at 0° Angle of Attack, M=1.56

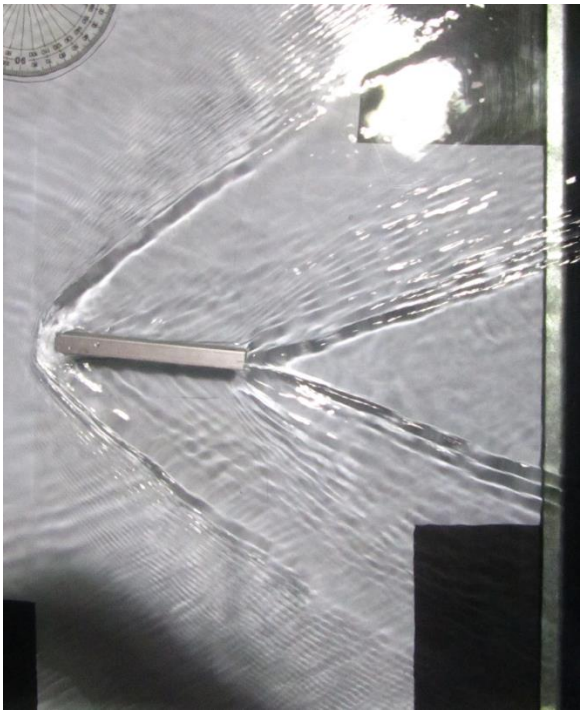

(a) Water table photograph

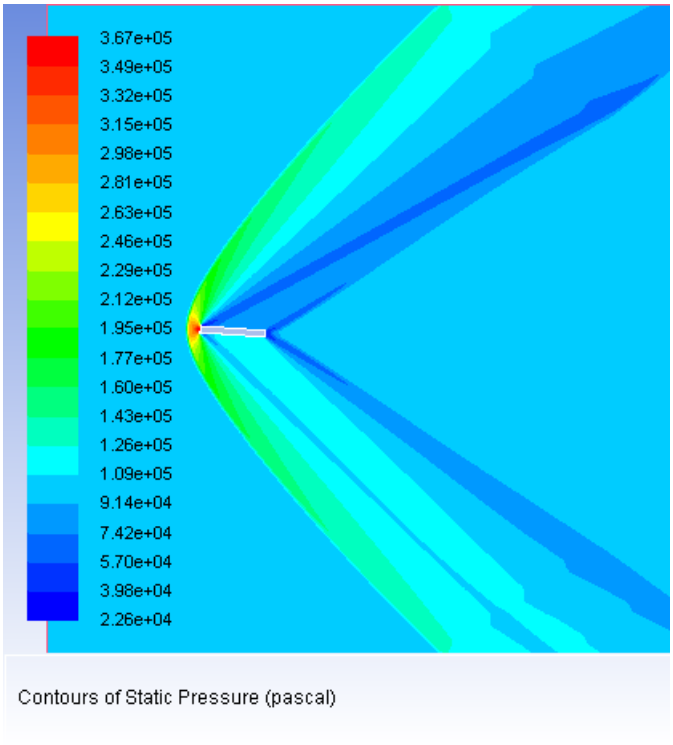

(b) CFD result showing static pressure

Figure 22– Case 2: Flat plate at 4° Angle of Attack, M=1.56

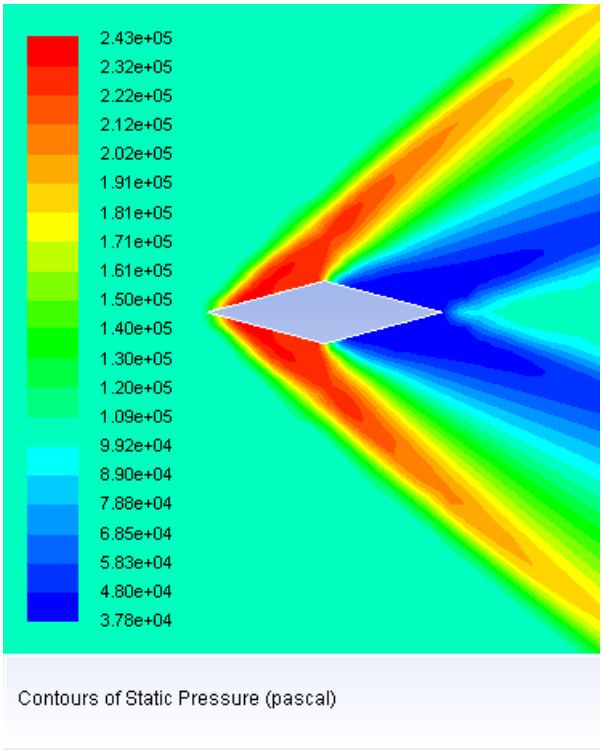

(c) Water table photograph (d) CFD result showing static pressure

Figure 23 – Case 3: Supersonic diamond at 0° Angle of Attack, M=2.2

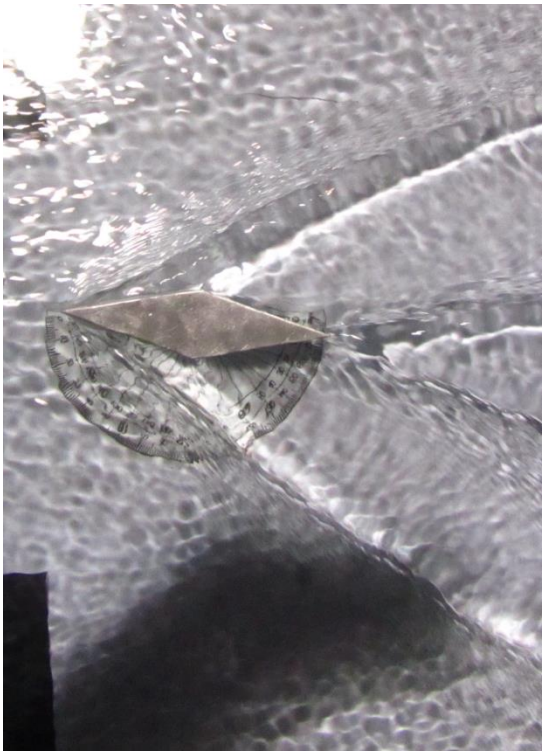

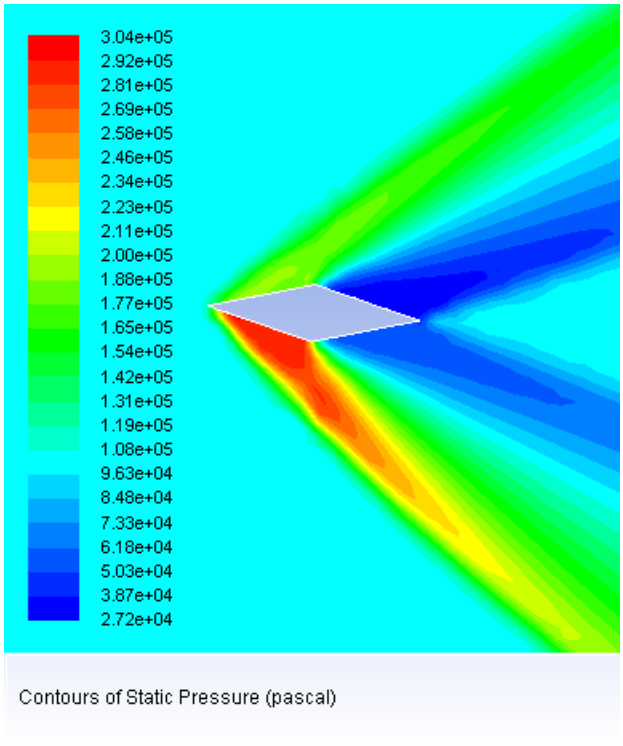

(a) Water table photograph (b) CFD result showing static pressure

Figure 24 – Case 4: Supersonic diamond at 4° Angle of Attack, M=2.2

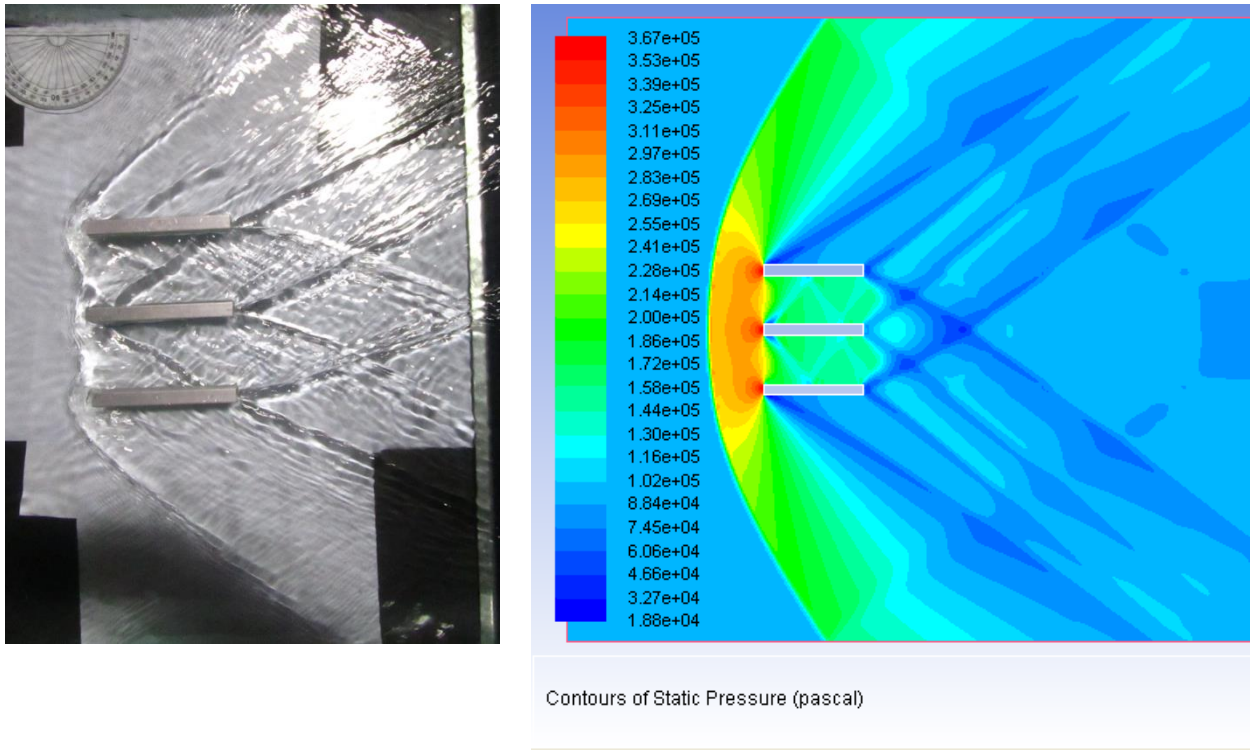

(a) Water table photograph (b) CFD result showing static pressure

Figure 25– Case 5: Flat plate cascade at 0° Angle of Attack, M=1.56

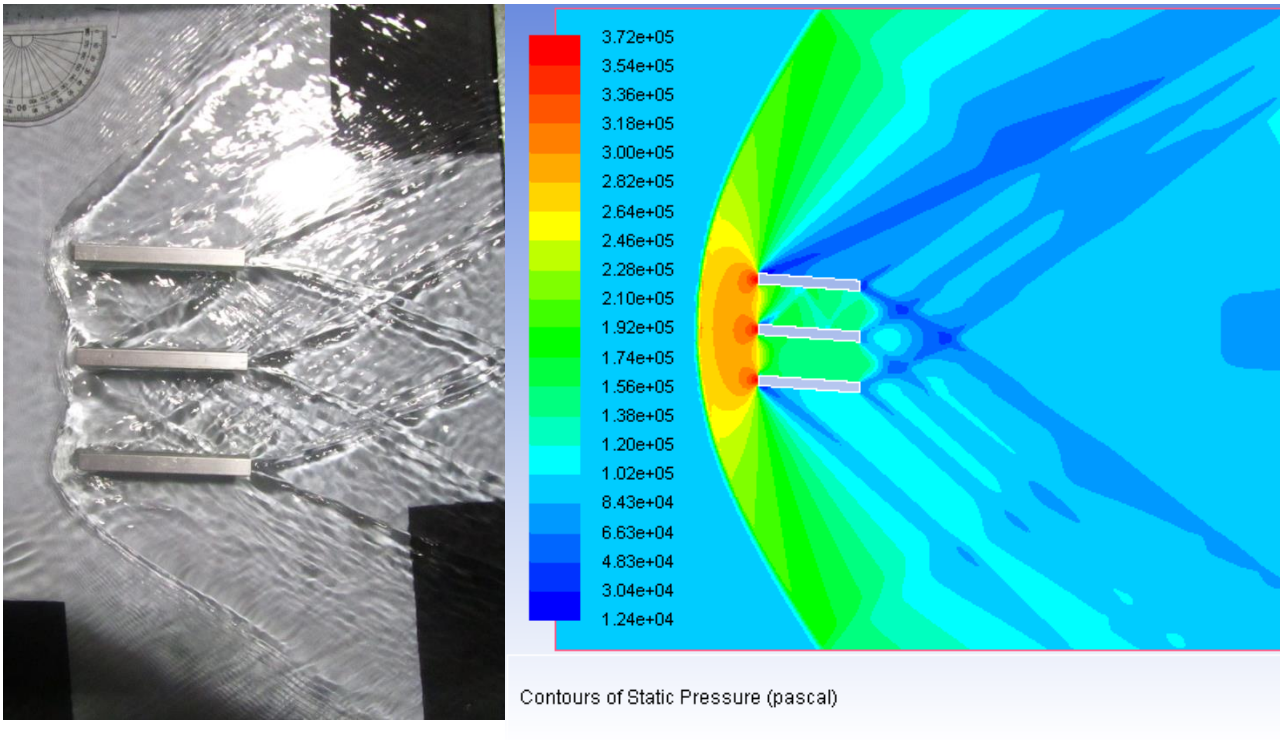

(a) Water table photograph (b) CFD result showing static pressure

Figure 26 – Case 6: Flat plate cascade at 4° Angle of Attack, M=1.56

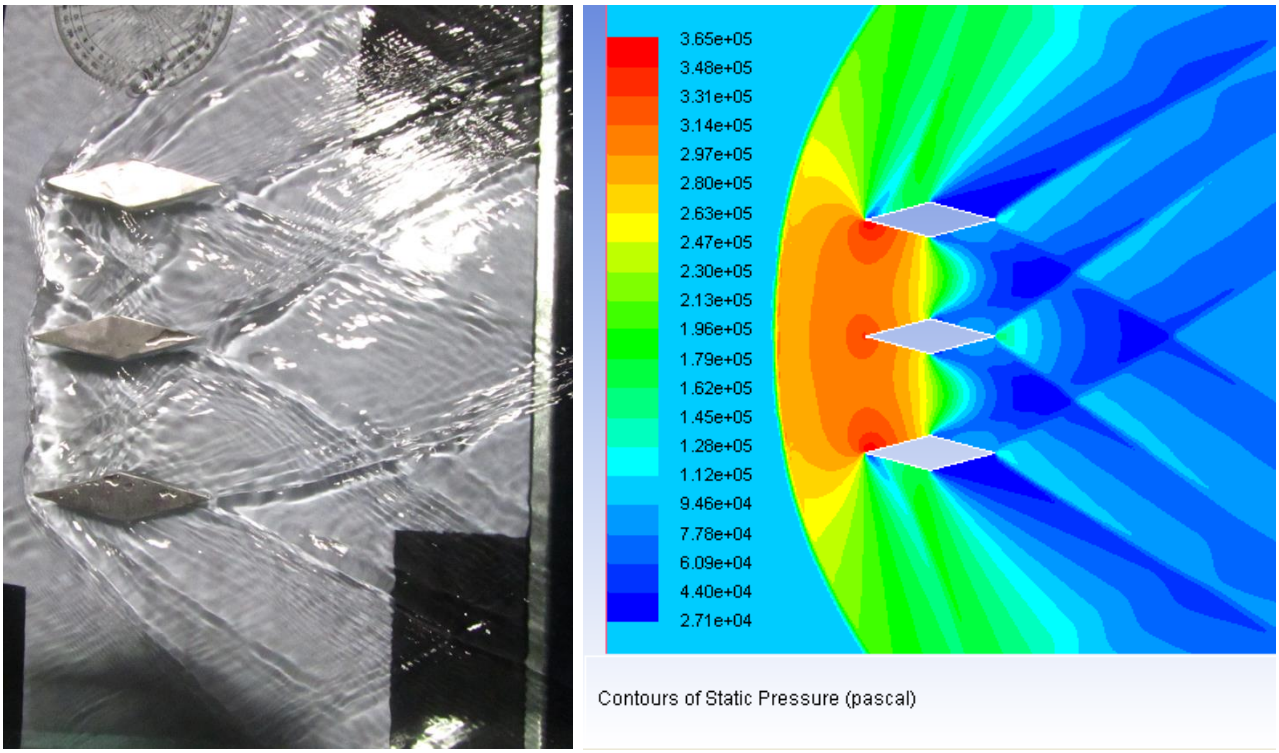

(a) Water table photograph (b) CFD result showing static pressure

Figure 27 – Case 7: Supersonic diamond cascade at 0° Angle of Attack, M=1.56

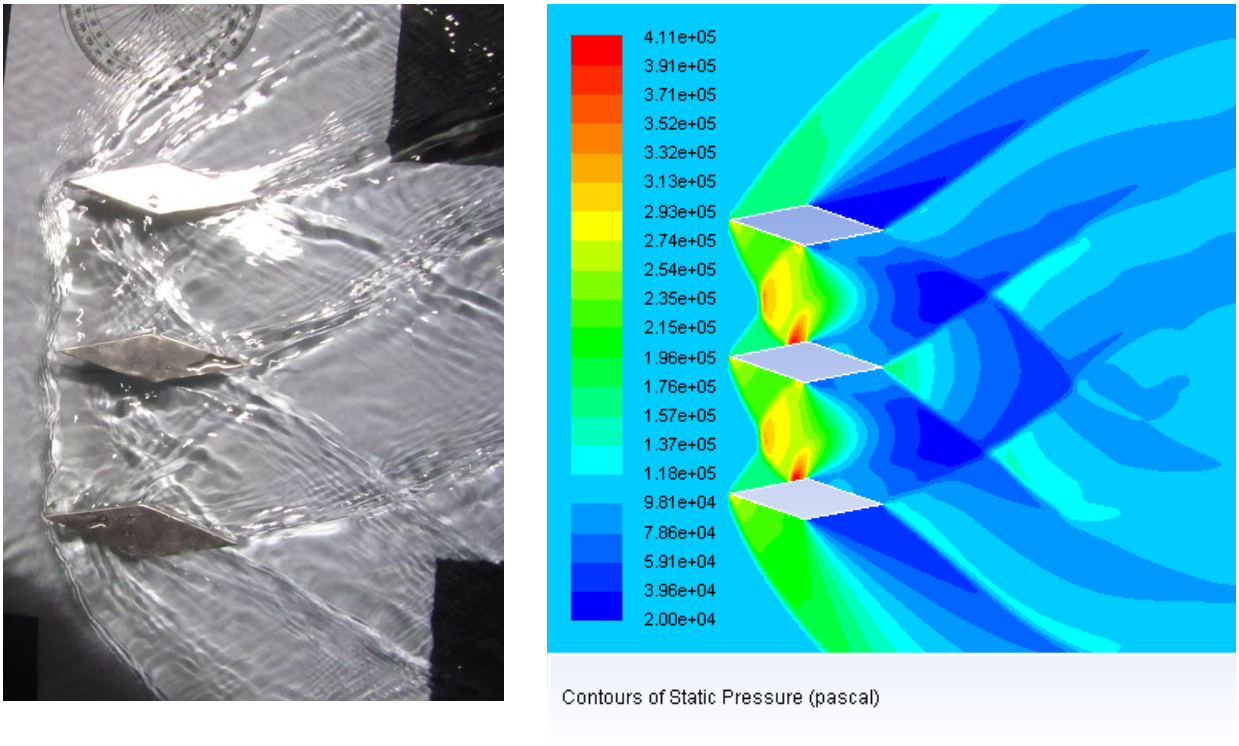

(a) Water table photograph (b) CFD result showing static pressure

Figure 28 – Case 8: Supersonic diamond cascade at 4° Angle of Attack, M=1.56

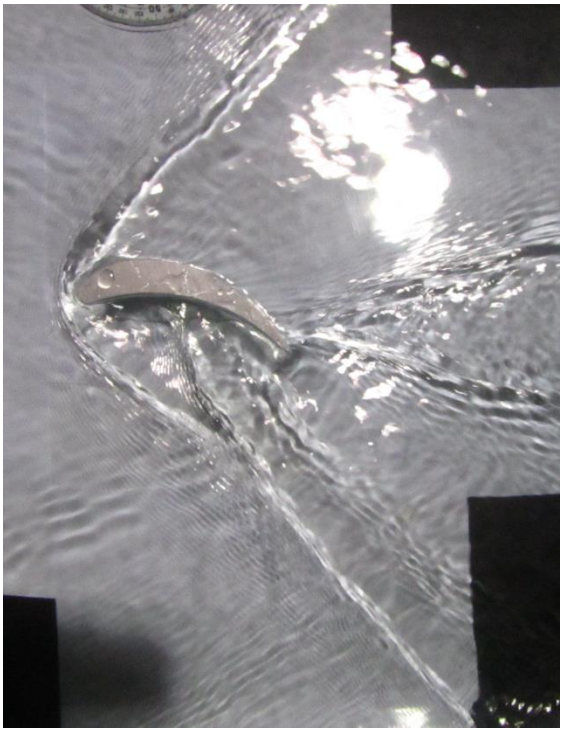

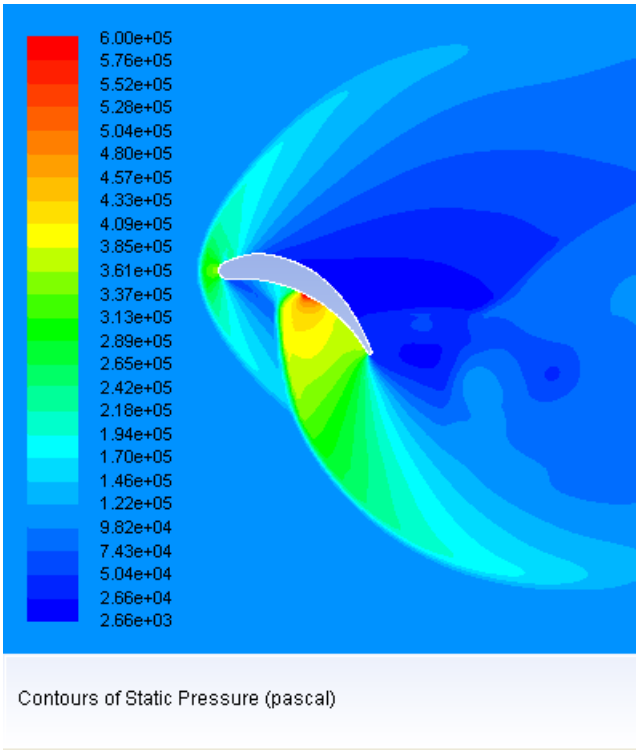

(a) Water table photograph (b) CFD result showing static pressure

Figure 29 – Case 9: Turbine blade 0° Angle of Attack, M=1.56

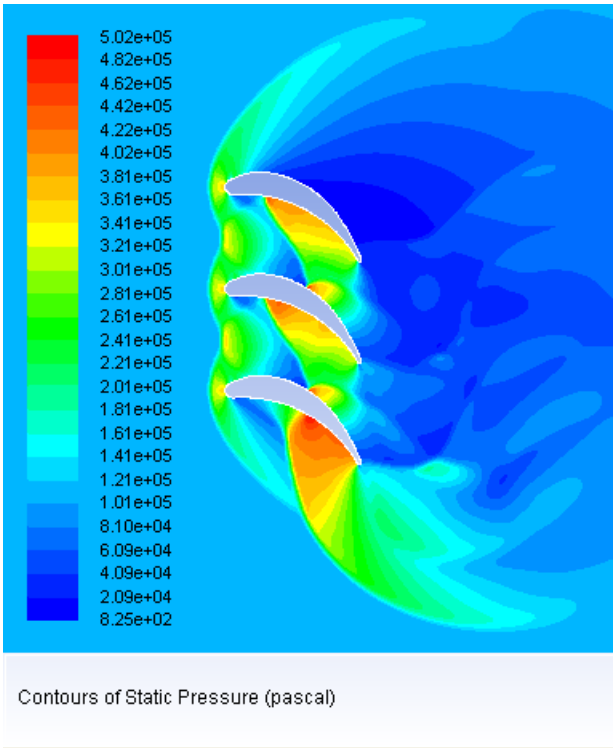

(a) Water table photograph (b) CFD result showing static pressure

Figure 30– Case 10: Turbine blade cascade at 0° Angle of Attack, M=1.56

Table 5 -Angles of the Bow Shocks of the Three Methods: Top refers to the bow shock that forms above the airfoil, and Bottom refers to the bow shock that forms below the airfoil.

			Angle Measurments (°)		
Case #	**Description**	**Shock Location**	**Analytical**	**Experimental**	**Computational**
1	Flat Plate 0° AOA	Top	40.5	41	42.90
		Bottom	40.5	41	43.34
2	Flat Plate 4° AOA	Top	38.87	40	43.71
		Bottom	44.5	45	45.00
3	Diamond 0° AOA, M=2.2	Top	41	31	41.46
		Bottom	41	33	41.11
4	Diamond 4° AOA, M=2.2	Top	37	26	37.39
		Bottom	46.5	35.5	46.03

Table 6 - Percent Error of the Three Methods: Error greater than ±10% is high-lighted yellow.

			% Error		
Case #	**Description**	**Shock Location**	**Analytical vs Experimental**	**Analytical vs Computational**	**Experimental vs Computational**
1	Flat Plate 0° AOA	Top	1.2%	5.9%	4.6%
		Bottom	1.2%	7.0%	5.7%
2	Flat Plate 4° AOA	Top	2.9%	12.5%	9.3%
		Bottom	1.1%	1.1%	0.0%
3	Diamond 0° AOA, M=2.2	Top	-24.4%	1.1%	33.7%
		Bottom	-19.5%	0.3%	24.6%
4	Diamond 4° AOA, M=2.2	Top	-29.7%	1.1%	43.8%
		Bottom	-23.7%	-1.0%	29.7%

DISCUSSION

To get a good sense of what value of error is acceptable, an uncertainty calculation is performed to find the fractional error.

The equation to find the Mach number from the water table experiment is shown below.

$$M = \frac{1}{sin\beta} \qquad (4)$$

The formula for uncertainty is seen below.

$$u_M = \sqrt{\left(\frac{\delta M}{\delta \beta}\Delta\beta\right)^2} \qquad (5)$$

After taking the partial derivative of Equation (4), the uncertainty equation for the Mach number is derived.

$$u_M = \frac{cos\beta}{\sin^2\beta}u_\beta \qquad (6)$$

The uncertainty of measuring the shock angle in the experiment is shown below. The shock angle found analytically for the flat plat is used in this calculation.

$$u_\beta = 5°, \beta = 40.5°$$

The uncertainty is calculated. The Mach number can be rewritten including the uncertainty.

$$u_M = 0.1618$$

$$M = 1.56 \pm 0.1618$$

With the uncertainty of the Mach number calculated, the fractional error of the Mach number can also be found. The number below was used as a guideline for acceptable angles.

$$Fractional\ Error = \frac{u_M}{M} = 10\%$$

Using the fractional error as a guideline for determining the acceptable error, most of the experimental and computational results match the analytical results for the flat plate cases within

the required 10%. The only discrepancy was on the top bow shock for Case 2 where the analytical and the computational had a positive error of 12.5% (shown in Table 6) which exceeds the allowable fractional error by 2.5%. This error could be due to CFD errors, like measuring the location of the shock in CFD.

With the current results, it is difficult to pinpoint the exact location of the shock. As seen in Figure 31, the shock locations are blurry and not easily defined. Shocks are abrupt discontinuities in the flow. In nature, this exists as an infinitesimally thin line. It is very difficult to capture a shock line that accurately represents nature in this way.

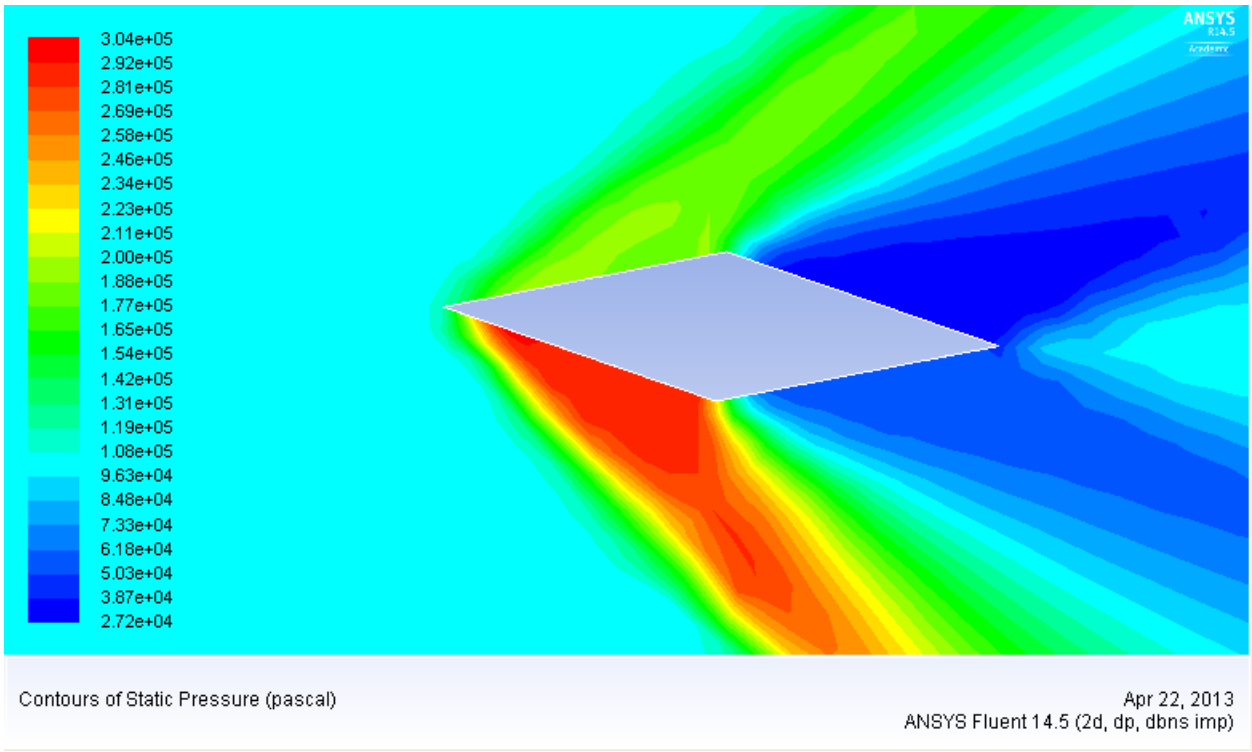

Figure 31 – Shock lines are not clearly defined

To capture the shock location clearly, the mesh in the shock region needs to be refined. A study was conducted at UNLV to determine the proper mesh for a shock line. Figure 32 below shows the results from the study (De Bues, Chen & Pepper, 2001). The shock line is blurry in the top picture. With mesh refinement, the shock location appears to be more precise. A mesh

refinement exhibited by the study conducted should be applied to future work in this area to get a more accurate result.

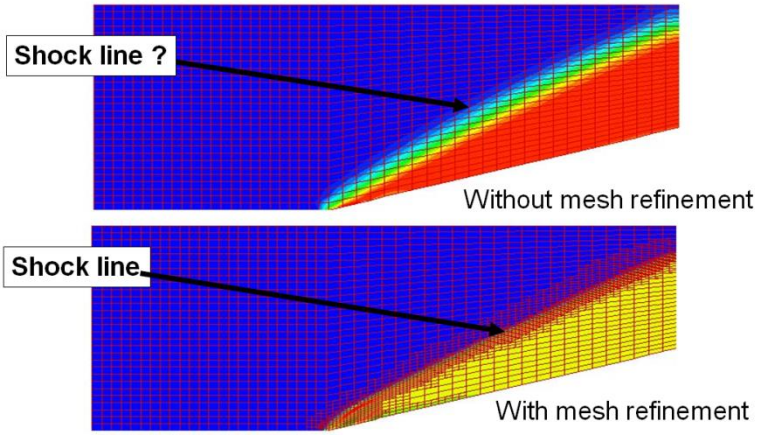

Figure 32 - Effects of Mesh Refinement at Shock Location (De Bues, Chen & Pepper, 2001)

Another source of error could come from the fact that the flat plate cases did not reach the convergence criteria of 1e-6 (Appendix B). The cases were stopped early due to time constraints. The angles were measured in CFD and were relatively close to the analytical value. Running the cases for longer time will smooth out some regions where the flow is not perfectly symmetric. However, it probably will not make much of a difference to the angle of the bow shock. More time is needed to run the cases to convergence. This should be done in future work. Examining Table 6 again, shows very high error for Cases 3 and 4 (supersonic diamonds) in the analytical and experimental and the experimental and computational comparisons. However, there is very small error in the analytical and computational comparison. This result suggests that the experimental results are inconsistent with the theoretical calculations as well as the computer modeling of the flow physics. Convergence issues are ruled out since both cases met the convergence criteria of 1e-6 (Appendix B). The fact that the error is within a range of about 20% to 40% and the signs are all consistent in each category suggests a systematic error. This systematic error could be due to the assumptions made in the water table experiment. It was

assumed that the shock lines shown in the experiment represent the oblique shock lines. The formula to calculate the angles of these shocks that was used in this experiment gives the angle of the Mach wave.

A Mach wave is similar to an oblique shock, but it is an infinitesimally weak oblique shock. That is why it is the limiting case for an oblique shock wave (Anderson, 2007). It is calculated by the formula below.

$$\mu = \sin^{-1}\frac{1}{M} \quad (7)$$

This formula is the same as the equation used to calculate the Froude number for a bow shock. This formula only applies to a shock at 0° deflection angle. This is when a weak oblique shock becomes a Mach wave (Pritchard, 2011). Using this formula implies that the shock formed in the experiment is a Mach wave instead of an oblique shock represented in the analytical and computational calculations. The water table analogy seems to break down for complicated flow scenarios.

The water table can be used as a general guideline for simple flow problems, such as the flat plate cases. Case 2 of the flat plate cases where the angle of attack is 4° should show the same type of problem as the supersonic diamond since it has a deflection angle of 4°. Since it is such a small deflection angle, there is not much discrepancy in the measured angle. The error is more prominent in the supersonic diamond cases because the deflection angle is quite large, up to 19°.

The cascade and turbine configurations (Cases 5-10) were tested in the water table and run in CFD, but they are not fully converged. Since they have not reached convergence, the results from these cases cannot be trusted as concrete results. However, they can be used as guidelines to how the flow is starting to form around each configuration. Figures 25-30 in the

Results section compare the water table results and the CFD results side by side. The water table results and the CFD results show similar trends.

Figures 25 and 26 show the flat plat cascades. Both the water table and the CFD show the shock diamonds that form after the airfoils. These figures also show that the shocks between the airfoils are reflected. However, the angles of the reflections and how many reflections occur are different. The shocks in the CFD are faint and difficult to locate. The CFD also predicts that a huge bow shock forms over all three of the airfoils. The CFD views the three airfoils as one object. The high pressure experienced at the leading edges of the airfoils blocks flow from entering in between the airfoils. This is why the shocks appear to be faint. The water table shows the reflected shocks more clearly than the CFD. Applying a denser mesh in front of the airfoils may smooth out the flow. Also a denser mesh between the airfoils where the reflected shocks occur will help shock lines become more apparent and easily measured. This should be done in the future.

Similar trends appear in Figures 27 and 28 with the supersonic diamond cascades. A huge bow shock forms before the three airfoils. As in the flat plate cascade cases, a denser mesh in front and between the airfoils is needed to smooth the flow. It should also be noted that more time is needed to converge these cases fully. Even with major errors, the water table and the CFD still show similar trends. Editing the mesh and running the CFD cases for a longer time should be done in future work.

The turbine blade cases in Figures 29 and 30 are interesting. The CFD for these cases is not fully converged. More time is needed to run these cases to convergence. Even with the convergence issue, the water table and the CFD also show similar trends. In Figure 29, the CFD shows the flow hitting the leading edge of the airfoil creating a detached bow shock. After the

shock, there is a small low pressure region on the lower surface of the airfoil where the flow is accelerated along the curved surface of the airfoil and creates a strong shock. This shock creates a region of high pressure represented by the red area long the bottom surface of the airfoil. This high pressure build up chokes the flow and makes the turbine less efficient. A higher total pressure ratio of the turbine means that the flow is more efficient, so more work can be extracted from it.

In the turbine cascade in Figure 30, the same characteristics appear in the cascade as in the single airfoil. The shock is seen to reflect off the surface of the airfoil. In a better turbine cascade design, the shock should be further downstream. This shock occurs too soon in the flow path creating a buildup of pressure that decreases the usefulness of the flow.

The water table results for Case 9 and 10 appear to be similar to the CFD results. The water table shows the bow shock on the single airfoil as well as the pressure buildup that occurs on the lower surface of the airfoil. The reflected shock is also seen in Figure 30a that corresponds to the buildup in the CFD result in Figure 30b. However, the CFD does not capture the wake behind the airfoil seen in both the single turbine blade as well as the cascade. This wake forms in the water table and is clearly seen by the hydraulic jump lines that form off the trailing edge. The inconsistent results could be due to the fact that turbulence was turned off in the CFD. Turning turbulence on in the CFD may allow wakes to form. Also, more time is needed to run the CFD cases. This will give more trusting results. Also more investigations into the usefulness of the water table are needed to finish the analysis. This should be done in the future studies.

CONCLUSION

This study shows that the shock angles from the analytical method and the computational method using CFD are fairly consistent for both the flat plate and the supersonic diamond cases. Experimental results differ slightly for the flat plate cases. This could be from the error that is associated with the shock location in the CFD not being clearly defined. The future work should refine the mesh in the shock locations. The experimental results for the supersonic diamond cases differed greatly from the analytical and CFD. This could be due to convergence issues, but mainly due to an error in assumptions for the oblique shock equations. Although the water table analogy breaks down for complex flows, it is still able to provide qualitative results that can be compared with the results from the CFD. Further investigation into possible discrepancies in the hydraulic jump analogy is required for the future work.

This thesis is able to prove that CFD and analytical results are consistent when the cases are allowed to run their full length to convergence. However, due to the scope of this project, some cases did not fully converge. More time is required to converge the cases in future analyses of this work.

REFERENCES

Anderson, Jr., J. D. (2007). *Fundamentals of aerodynamics*. (4th ed.). New York: McGraw Hill.

Bush, J., & Aristoff, J. (2008). *Hydraulic jumps*. Retrieved from http://math.mit.edu/~kasimov/fluid-mechanics/hydraulic-jump.html

De Bues, T., Chen, Y., & Pepper, D. W. (2001). *Hipsec review*.

Gallardo, J. G. (2010, Feb 26). *Fluent - Supersonic flow over a wedge*. Retrieved from https://confluence.cornell.edu/display/SIMULATION/FLUENT - Supersonic Flow Over a Wedge - Problem Specification

Culbreth, B. (2012). Hydraulic jump analogy to compressible flow shocks [Class Handout]. Department of Mechanical Engineering, University of Nevada, Las Vegas, Las Vegas, NV.

Martin, R., Forry, D., Maier, S., & Hans, C. (2012, Dec 7). *Ge's next 7fa gas turbine "test and validation"*. Retrieved from http://www.ge-energy.com/content/multimedia/_files/downloads/GEA18457A 7FA GI 7-27-11.pdf

Pritchard, P. J. (2011). *Fox and mcdonald's introduction to fluid mechanics*. (8th ed.). Hoboken: John Wiley & Sons, Inc.

Tu, J., Yeoh, G. H., & Liu, C. (2008). *Computational fluid dynamics: A practical approach*. Boston: Elsevier

APPENDIX A

Fluent Settings

The following steps were performed to model each case tested in this thesis. The case shown below is an example case that uses the same set up, but it has different geometry.

Workbench Instructions

1. Drag over Fluid Flow (Fluent) from the toolbox to the workspace.

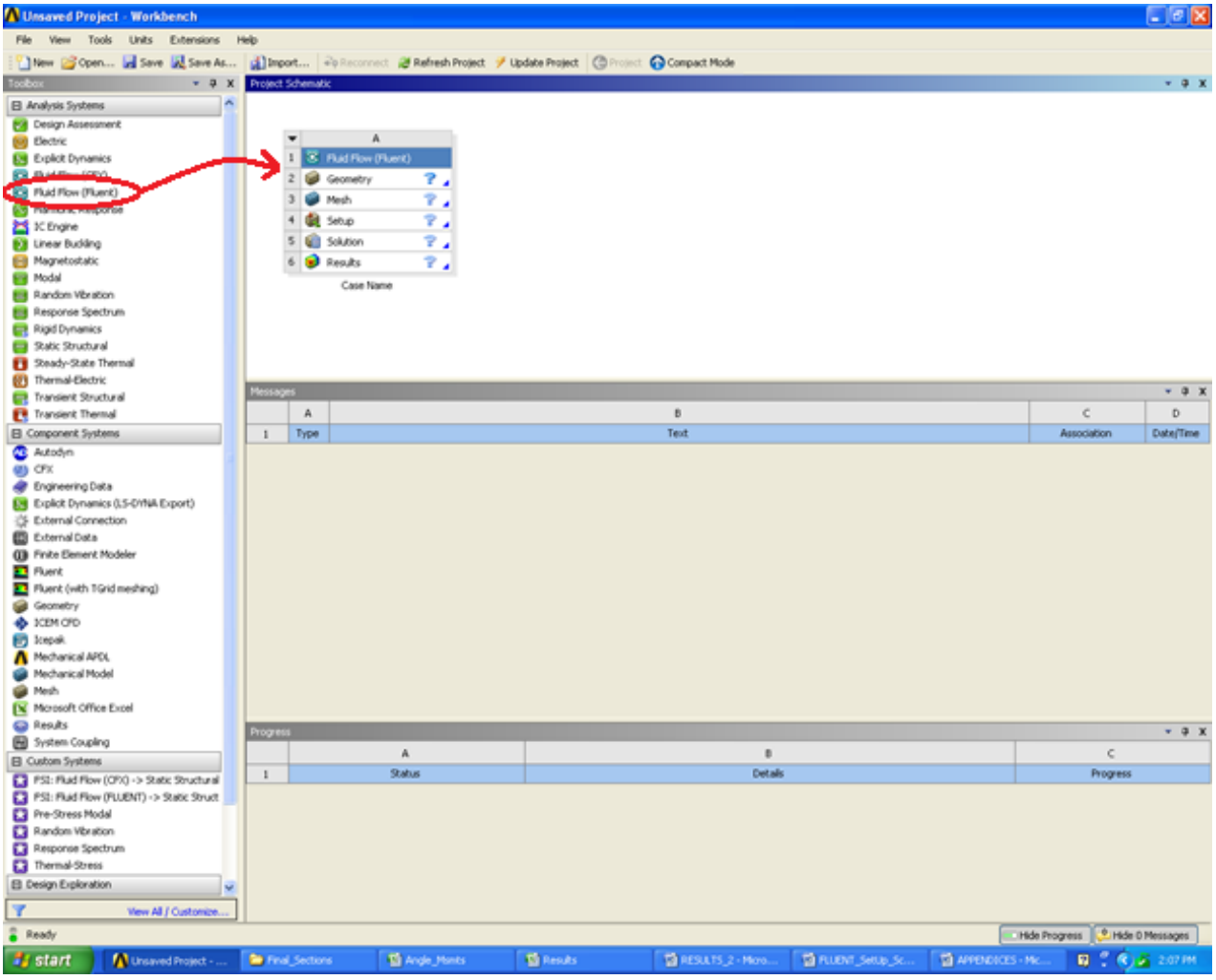

Geometry

1. Open the geometry tab.

2. Make sure the units are in millimeters.

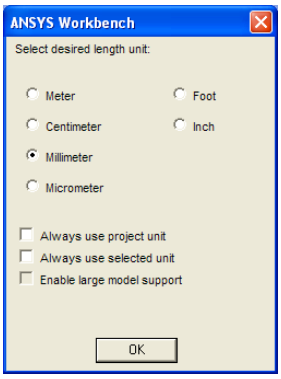

3. Create geometry of the fluid domain and airfoil. Specify the dimensions here.

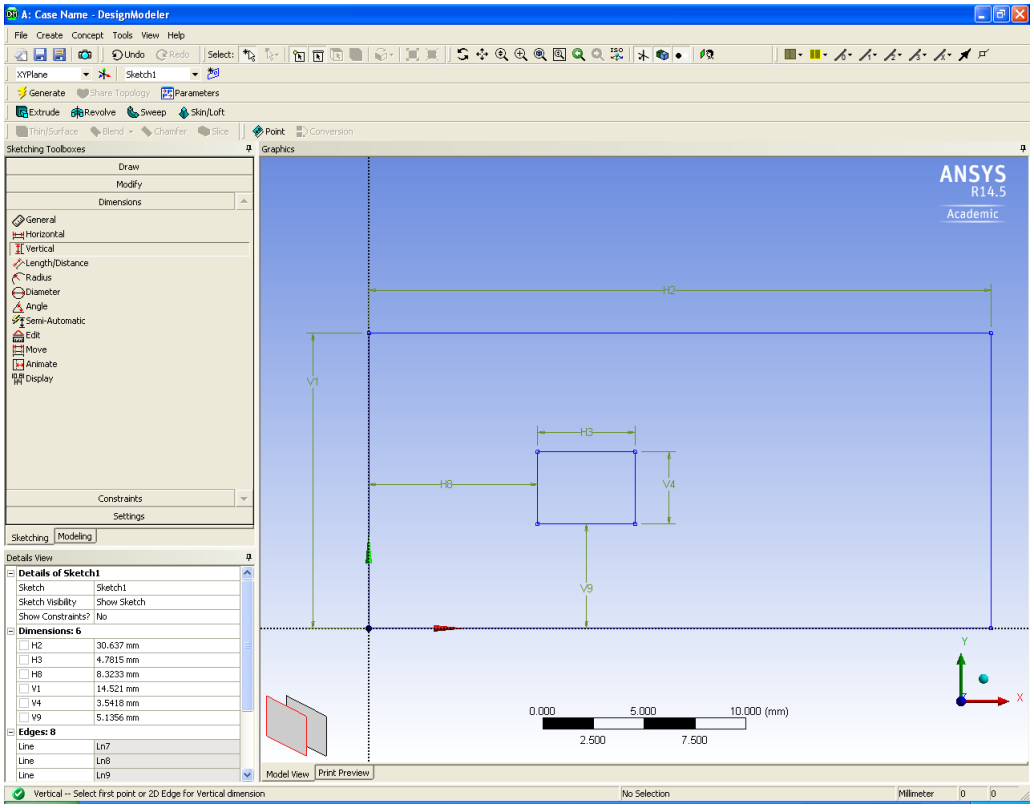

4. In the overhead menu, click on “Concept” and then “Surface from Sketches.” Select the outer edges of the fluid domain geometry using the edge tool. Click apply.

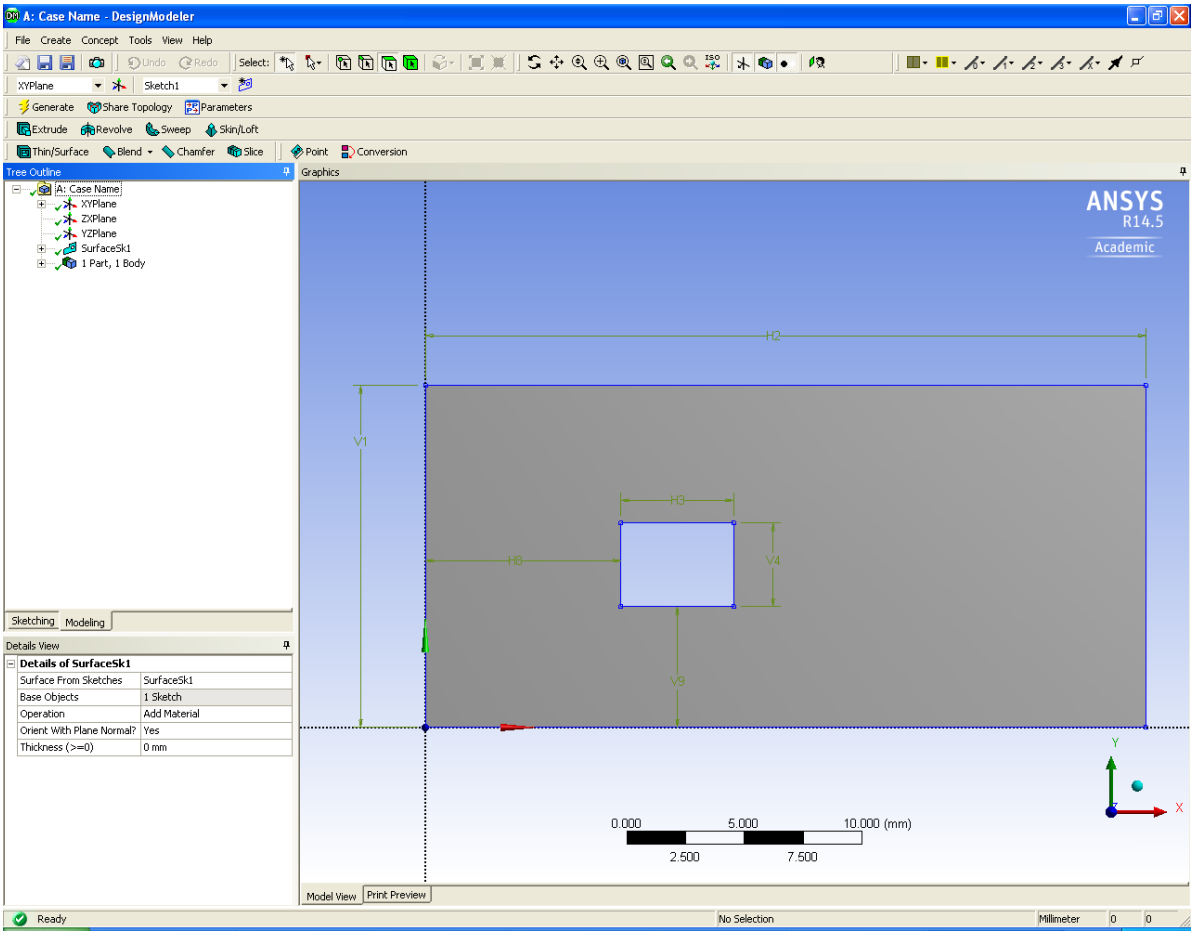

5. In the tree outline, open “Surface Body.” Go down to “Details of Surface” and change “Fluid/Solid” to “Fluid.”

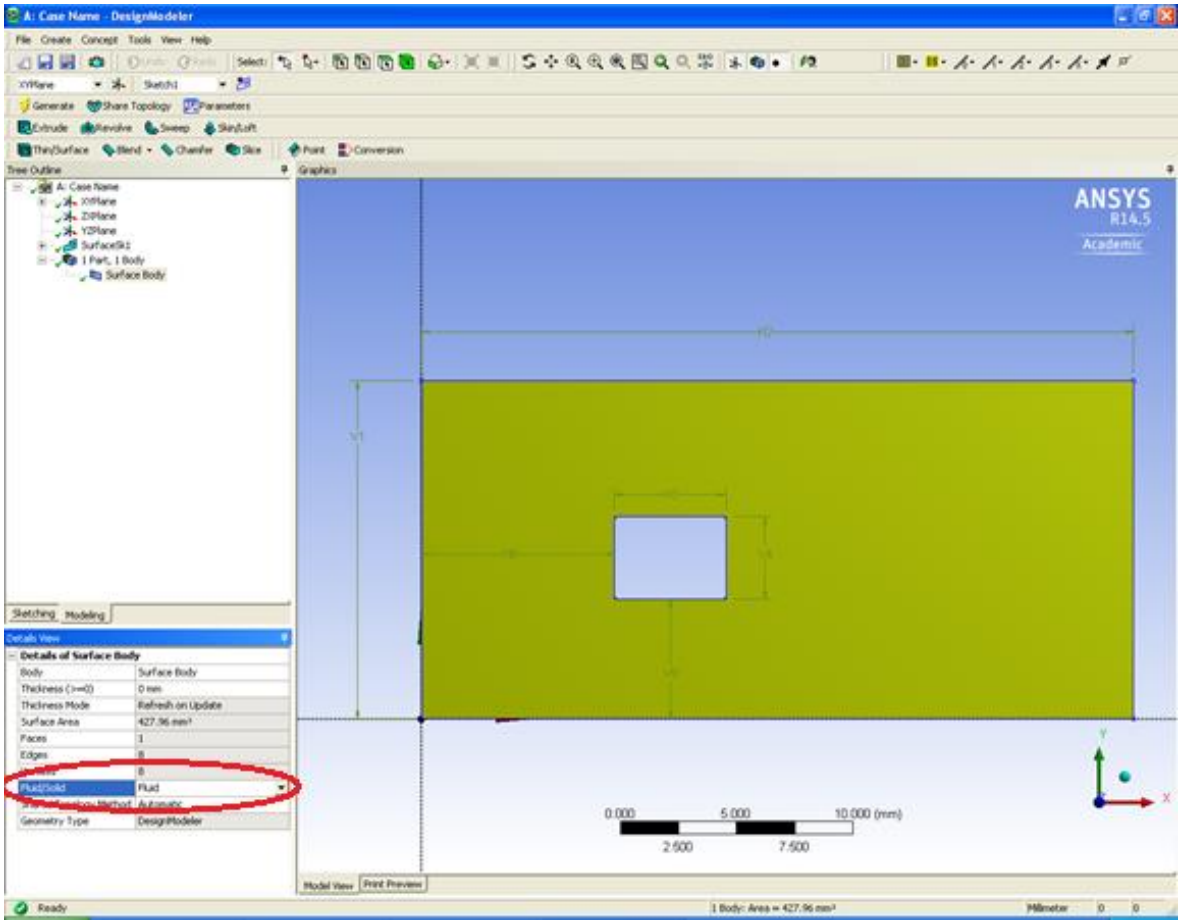

6. Save Project

Meshing

1. Open up the mesh creator from the workbench.

2. In the tree outline, right click on “Mesh.” Click on “Insert” and then “Sizing.”

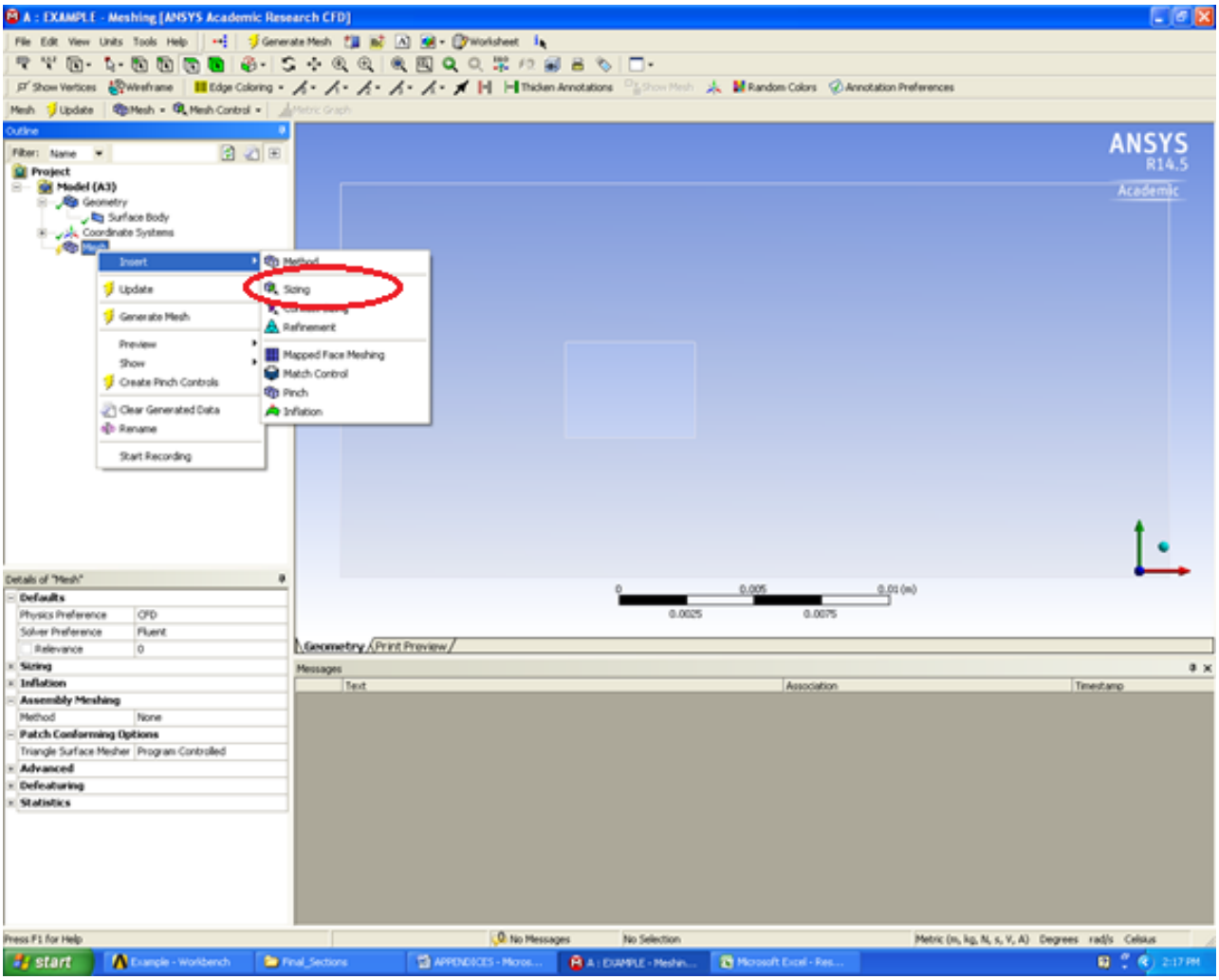

3. Select the face tool and click on the fluid domain. Change the element size to the required dimension and click “Apply.”

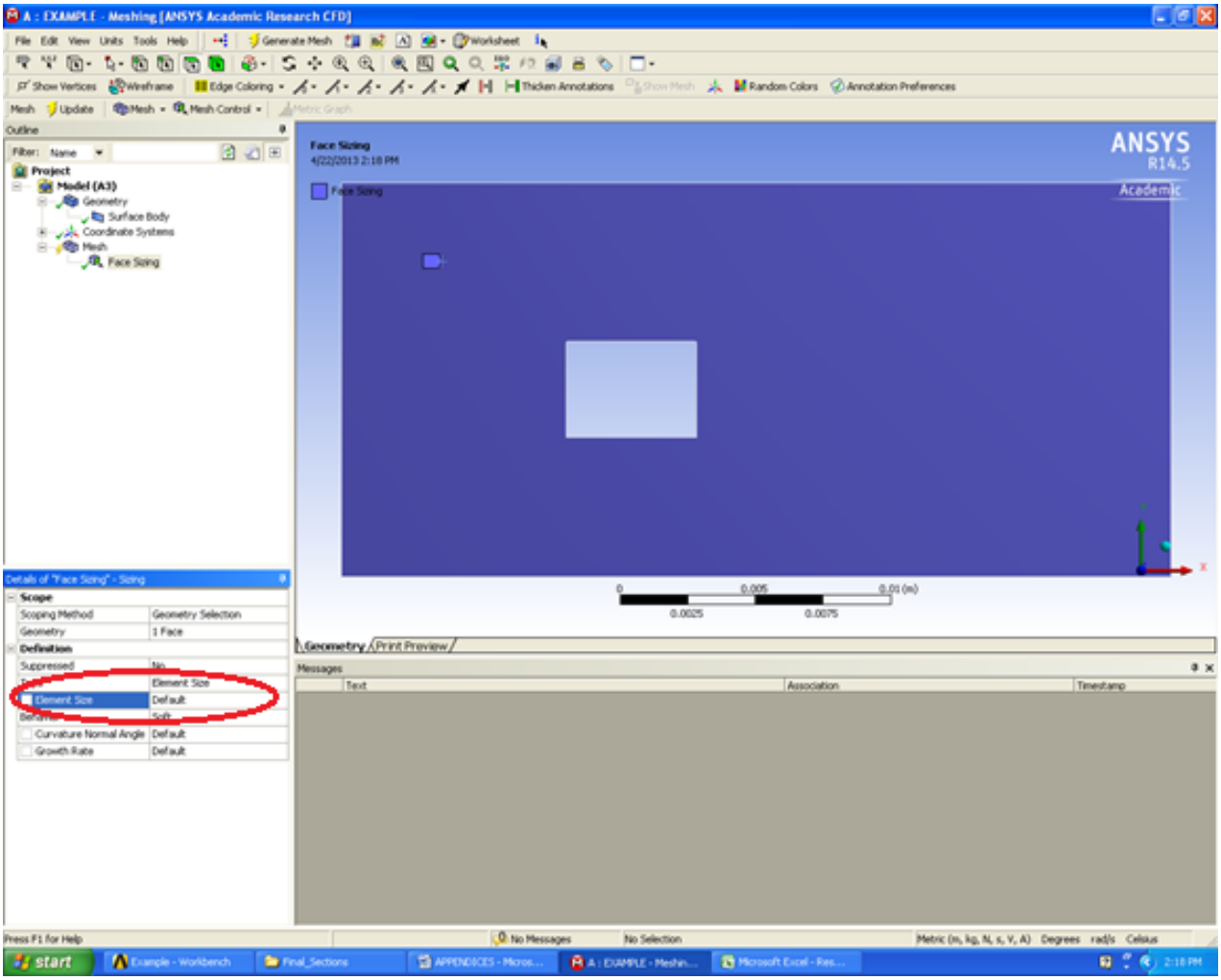

4. In the tree outline, right click on “Mesh.” Click on “Insert” and then “Refinement.”

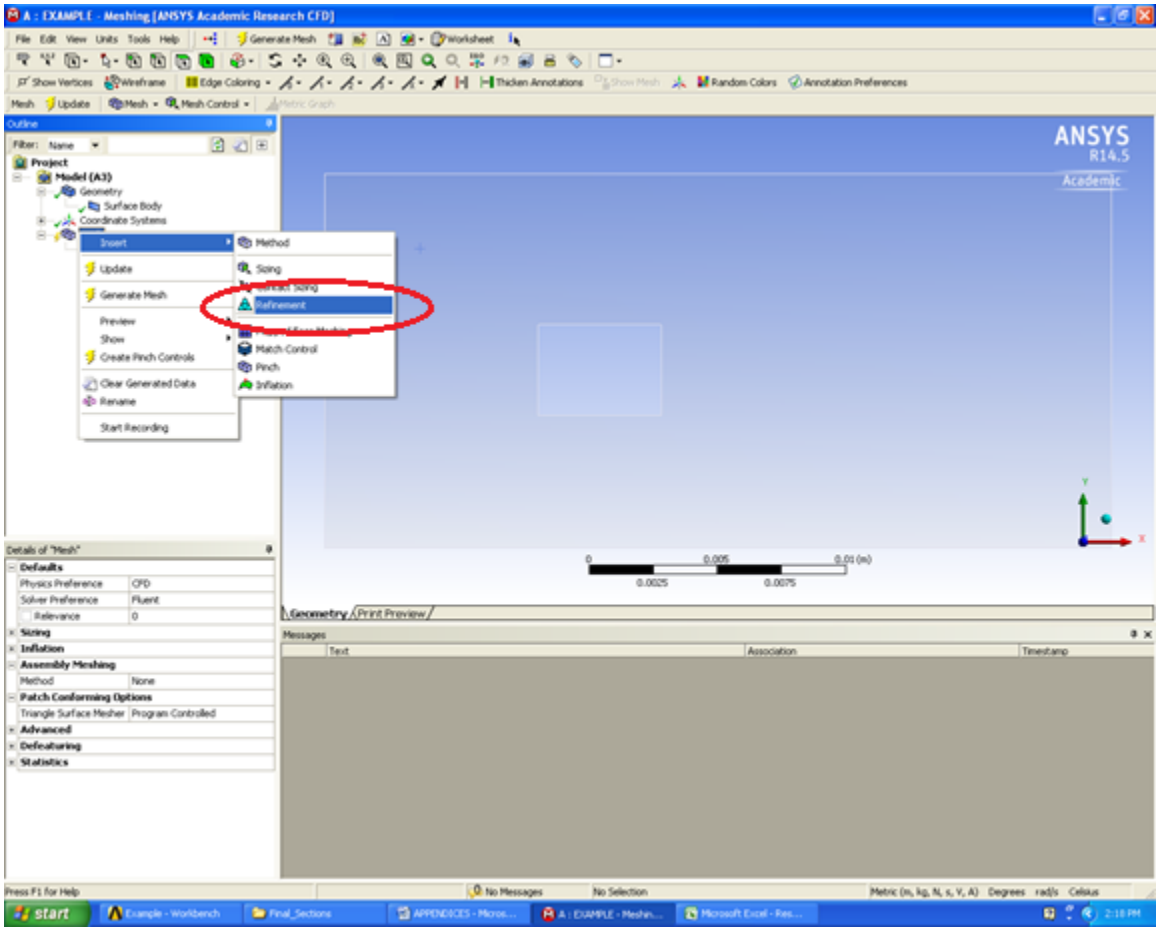

5. Select the edges of the airfoil geometry. Set the “Refinement Level” to 1 and click “Apply.”

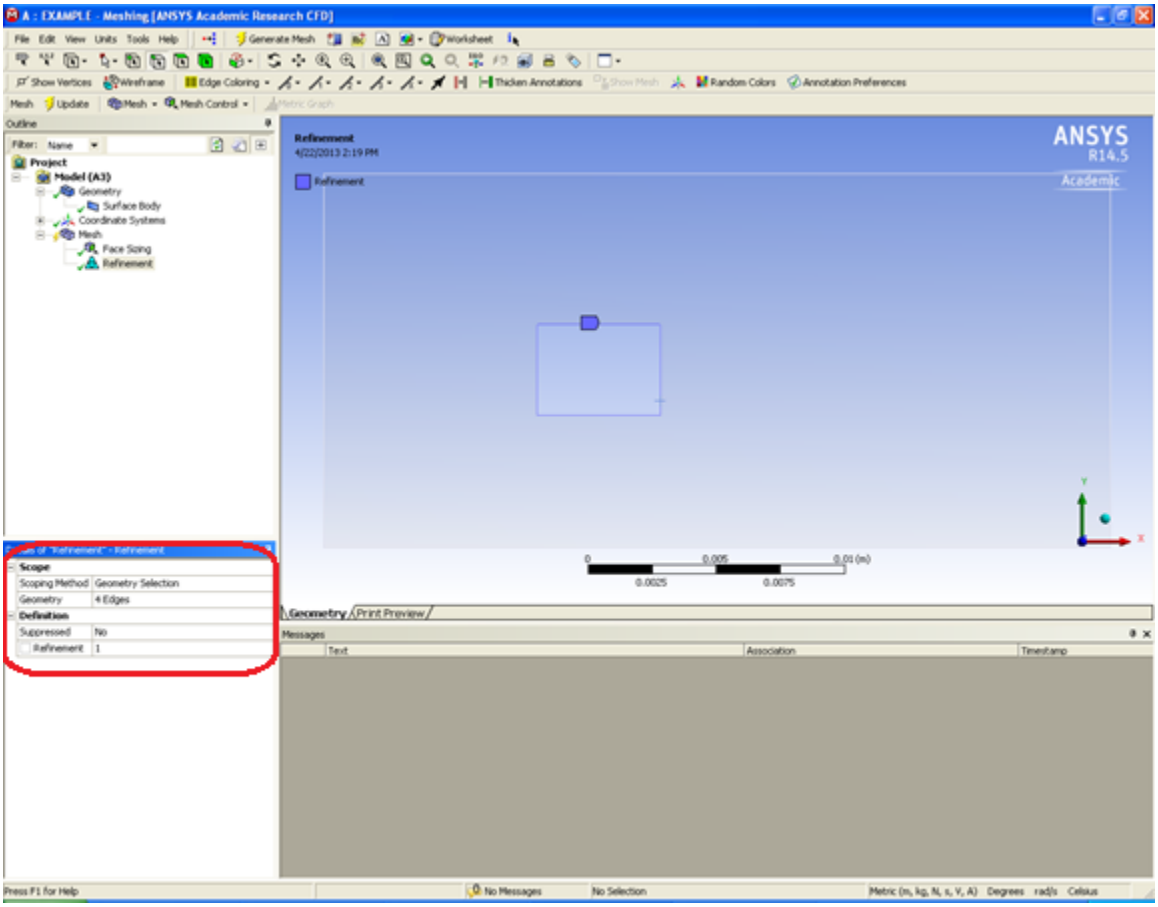

6. Click on “Generate.”

7. Select outer boundaries of the fluid domain using the edge too. Right click and select "Create Named Selection." Rename selection to "Farfield."

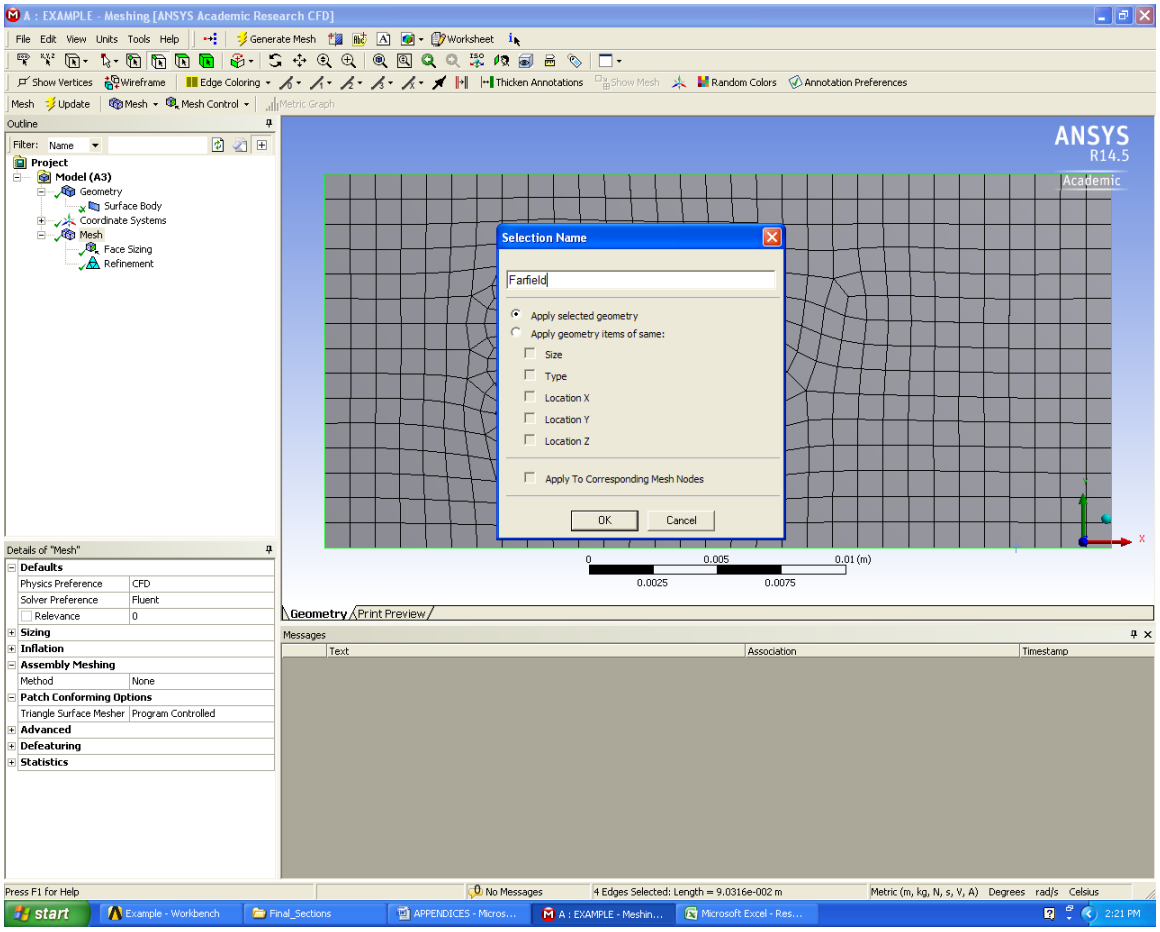

8. Select outer boundaries of the airfoil using the edge too. Right click and select “Create Named Selection.” Rename selection to “Walls.”

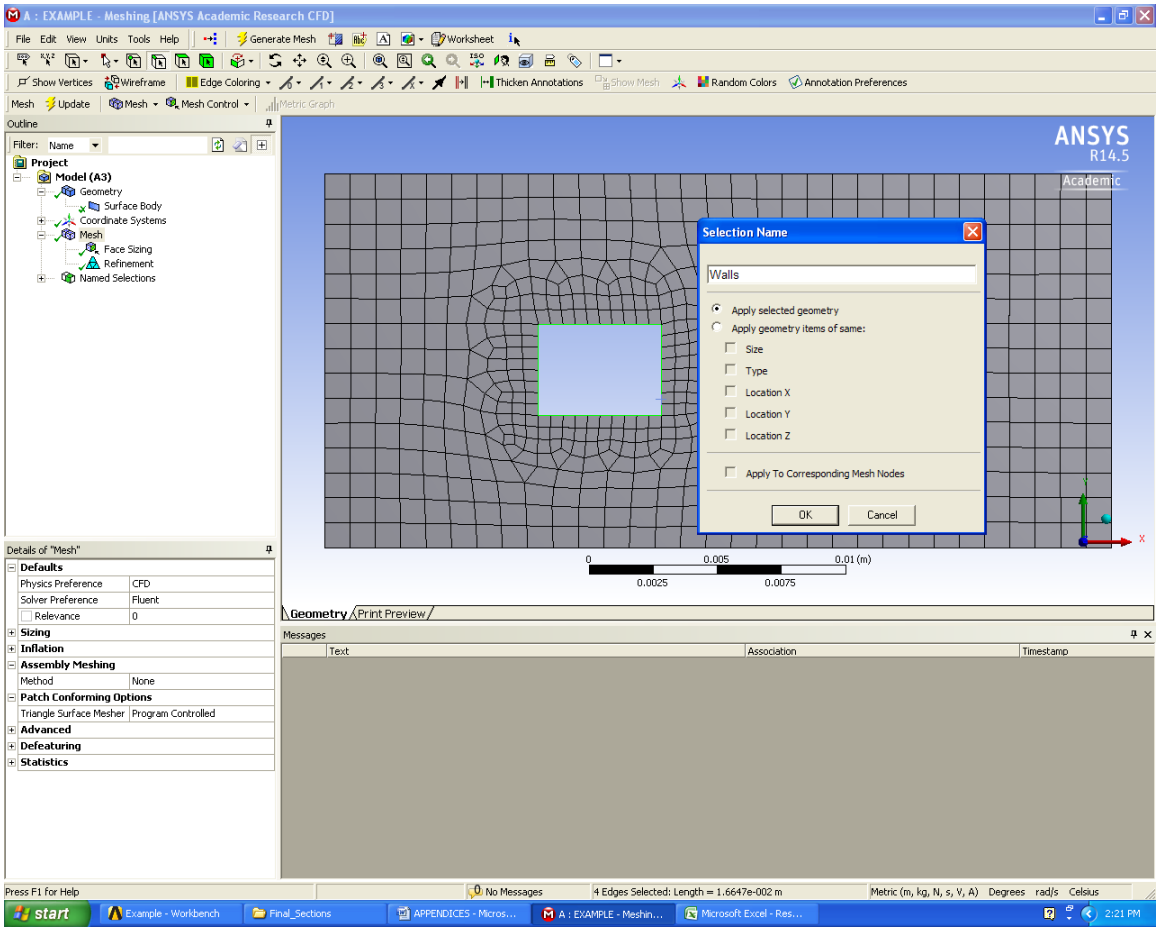

9. Click on “Update Project.”

Set-Up

1. From the Workbench, click on “Set-Up” to open it.
2. The Fluent Launcher opens. Make sure the “Dimension” is in 2D. Match the rest of the options to the following picture.

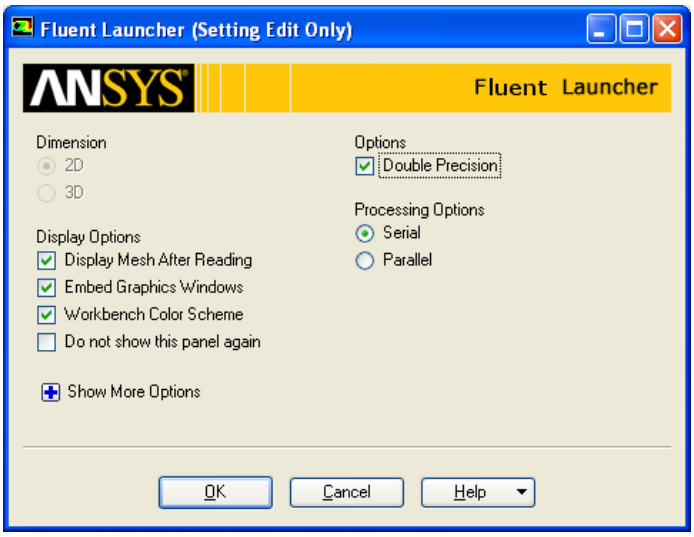

3. Under “General,” the following figure shows the settings used.

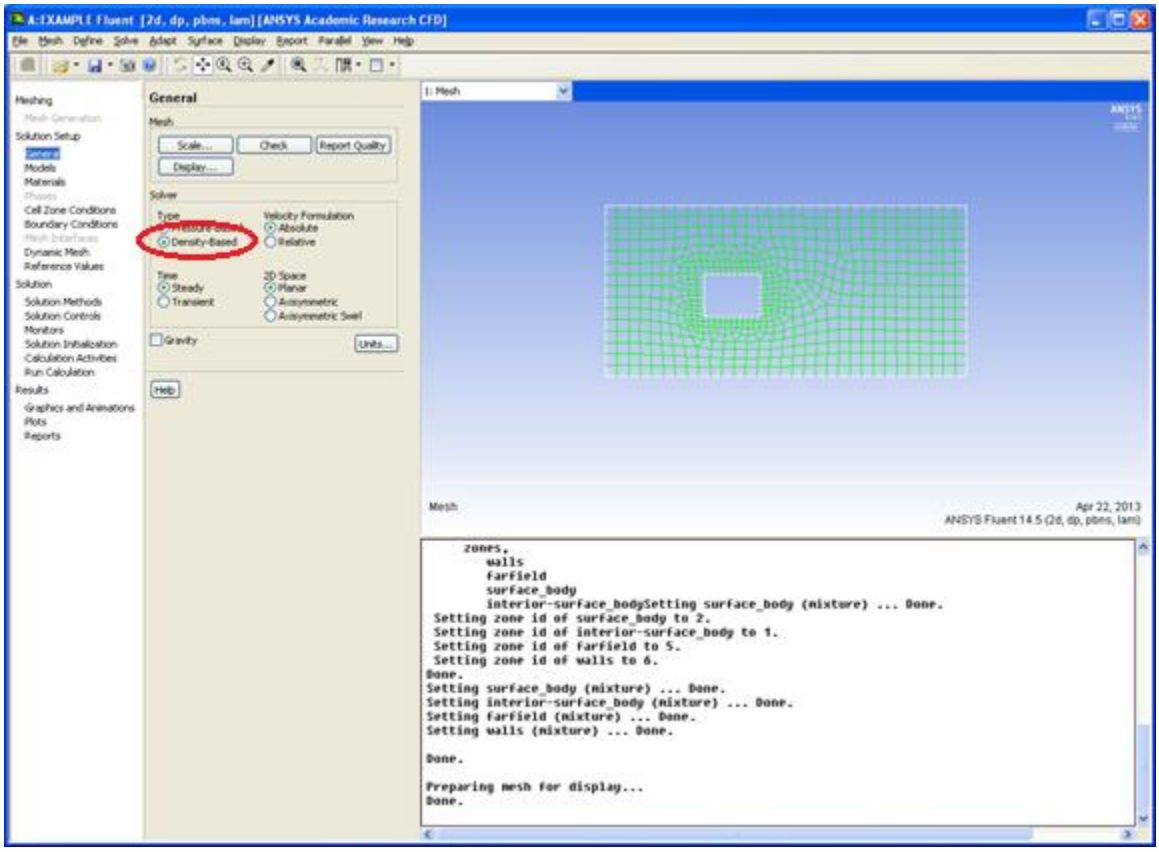

4. Under “Models,” make sure “Energy” is “On” and “Viscous” is set to “Inviscid.”

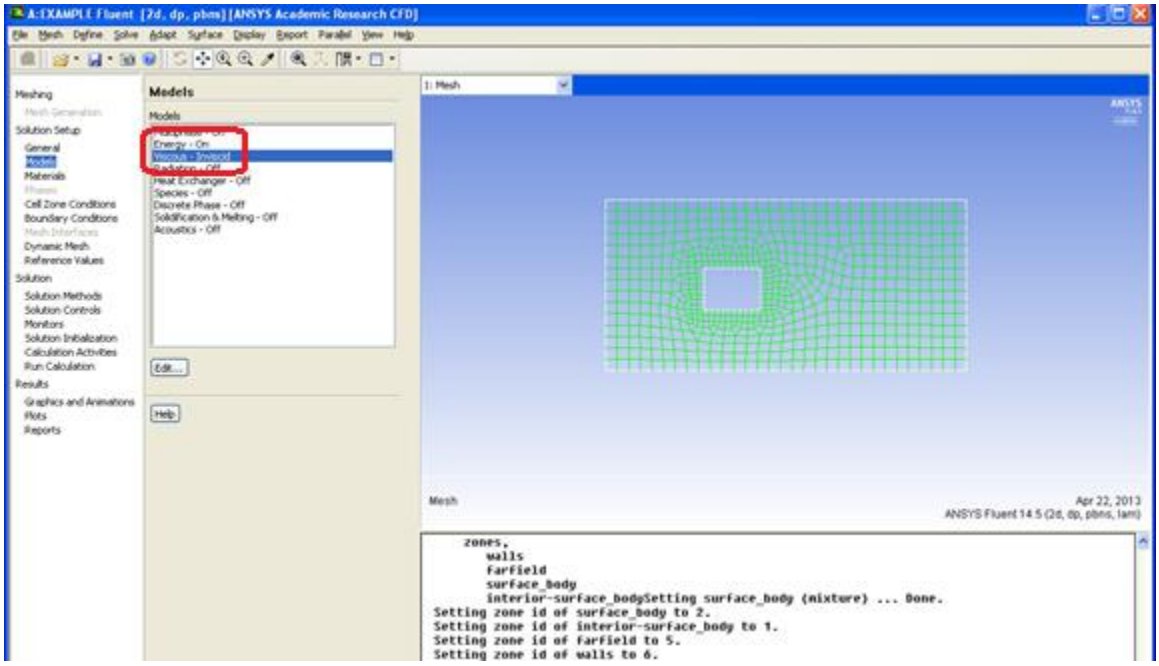

5. Under “Materials,” click to edit “Air.” Change the “Density” to “ideal-gas” in the pull-down menu. The rest of the values should change to match the following figure.

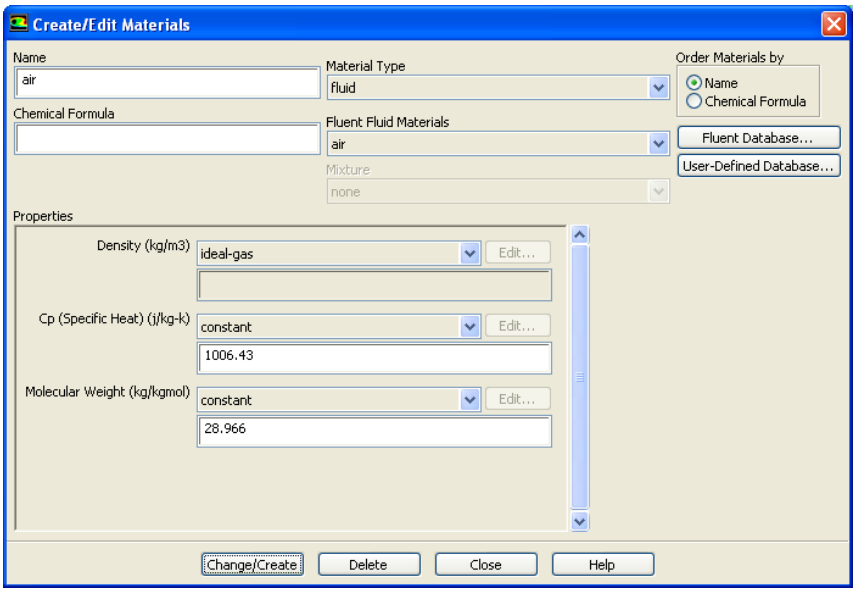

6. Under “Boundary Conditions,” change “Farfield” to have “Type” of “Pressure far-field.” In the “Pressure Far-Field,” window, change the “Gauge Pressure” and “Mach Number” to match the following figure.

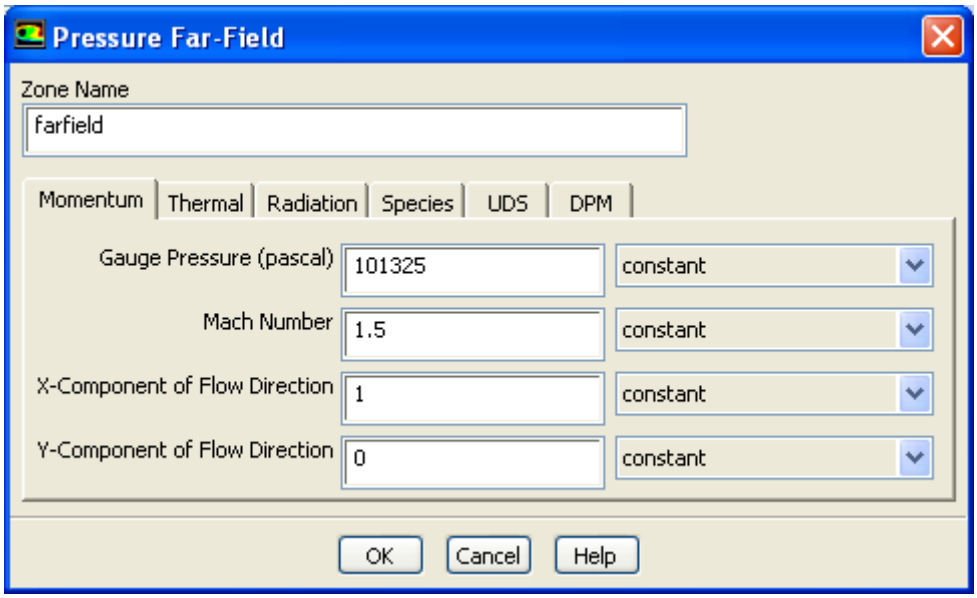

7. Still under the “Boundary Conditions” tab, click on “Operating Conditions.” Change the “Operating Pressure” to 0.

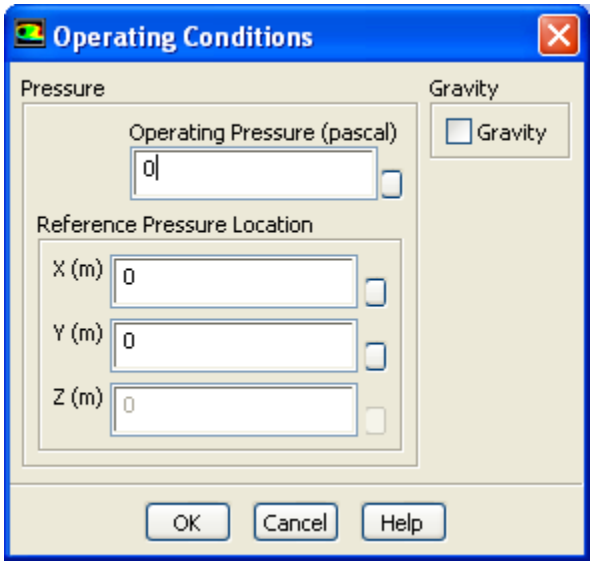

8. Under “Reference Values,” change “Compute from” to “Farfield.”

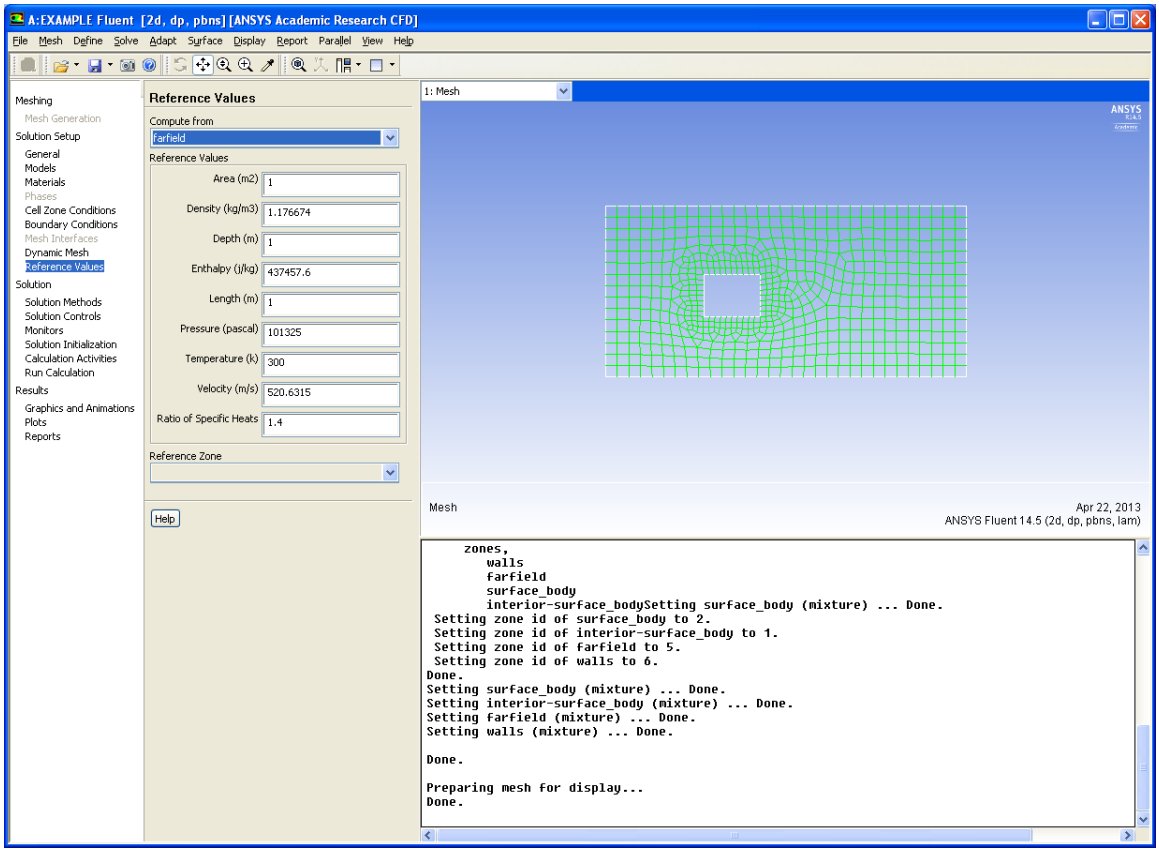

Solution

1. Click “Solution Methods” and match the options to the following figure.

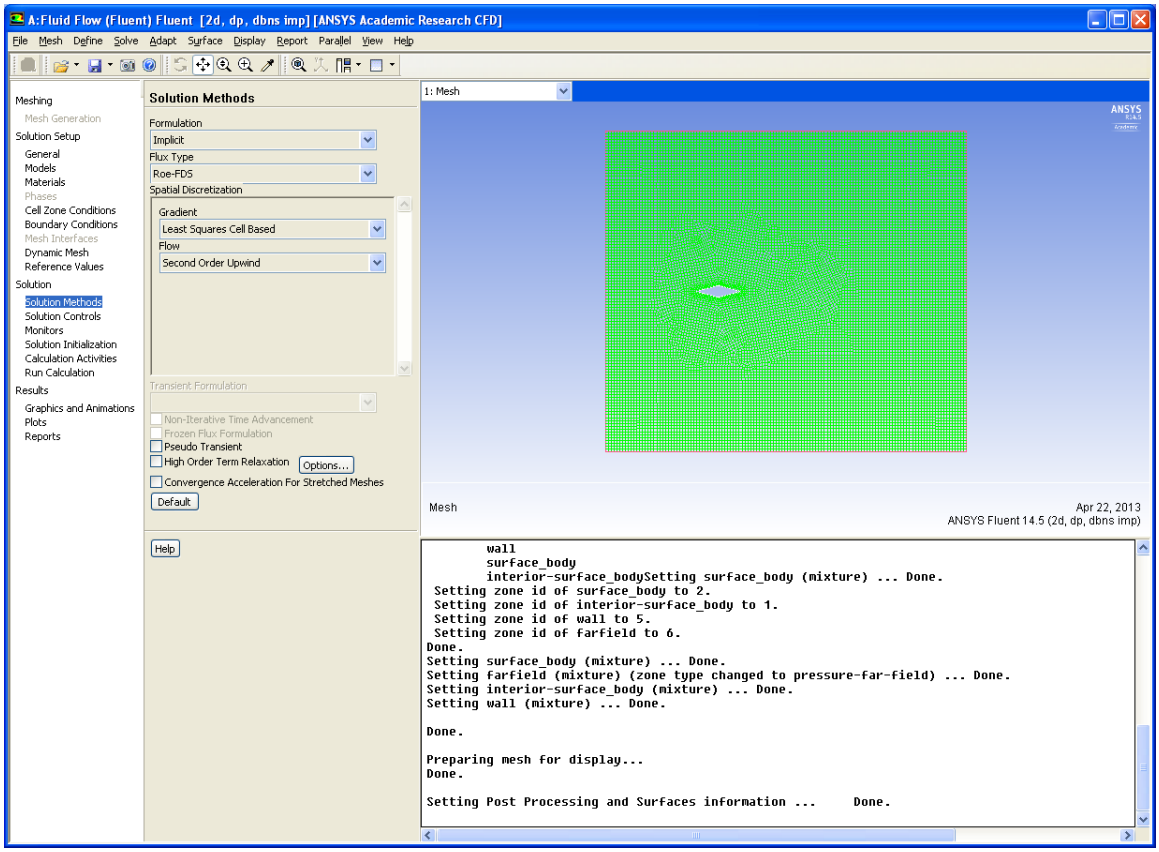

2. Under “Solution Controls,” change the “Courant Number” to 0.3.

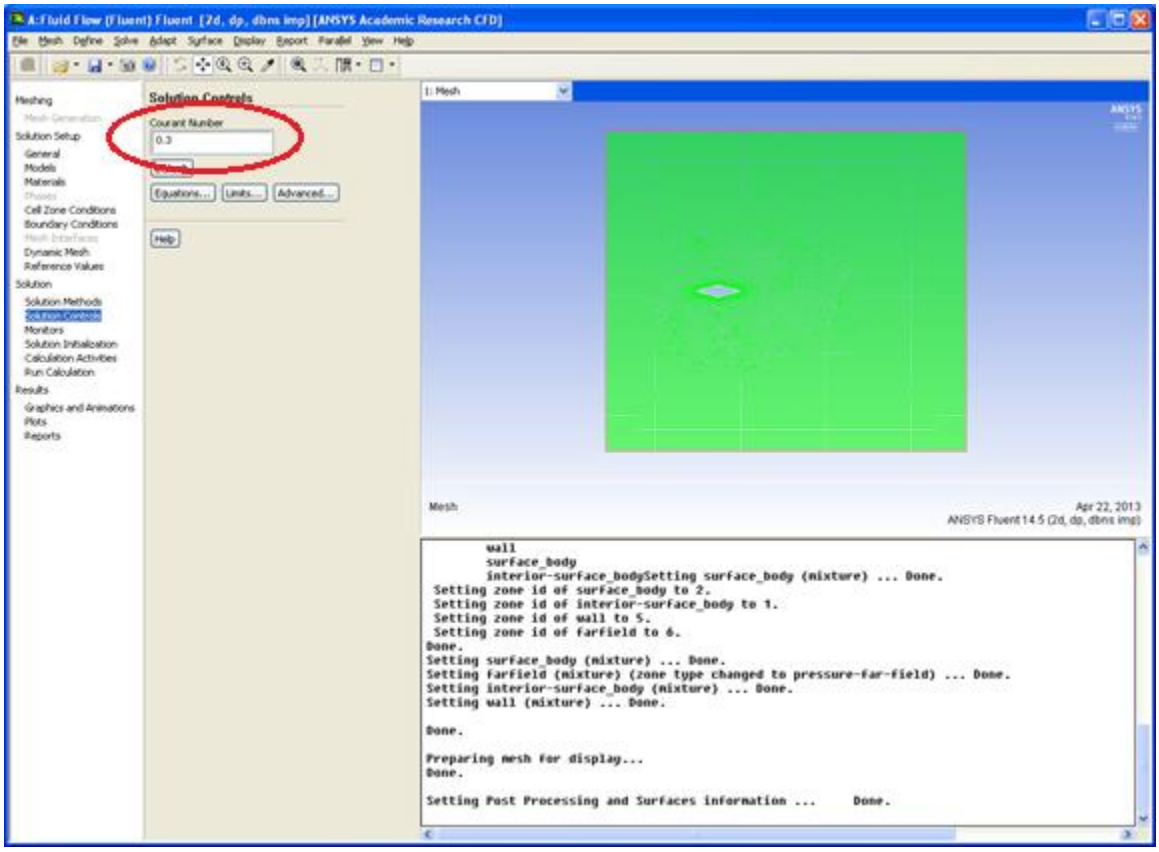

3. Under “Monitors,” change all the residuals to 1e-6.

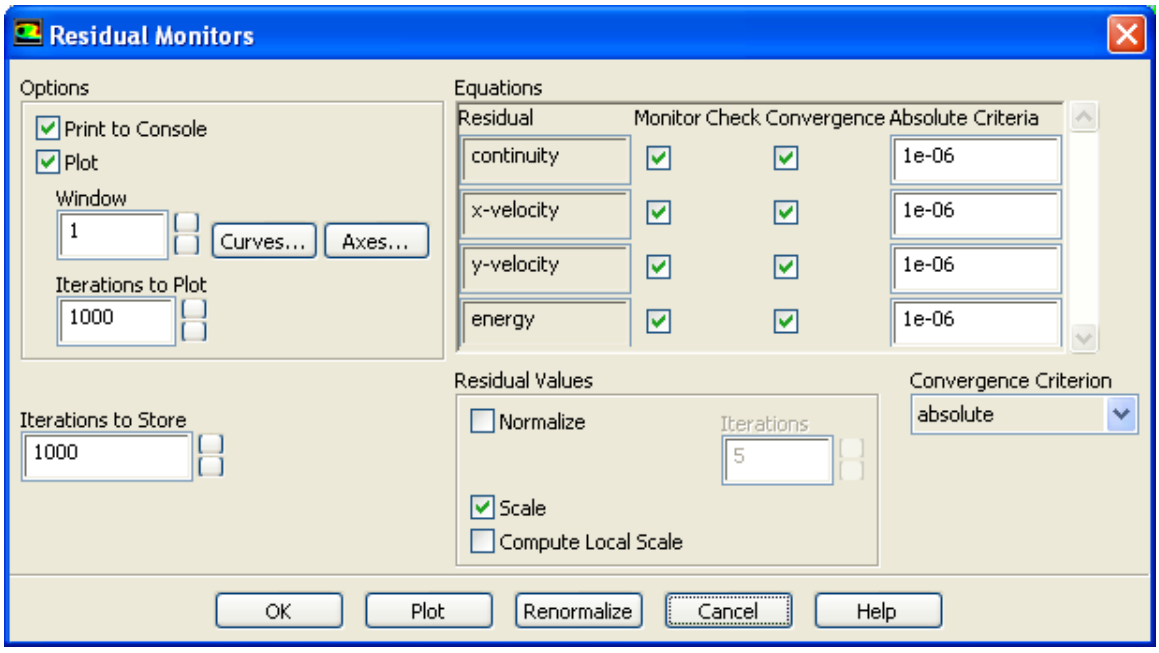

4. Initialize the solution by computing from “Farfield” in the “Solution Initialization.”

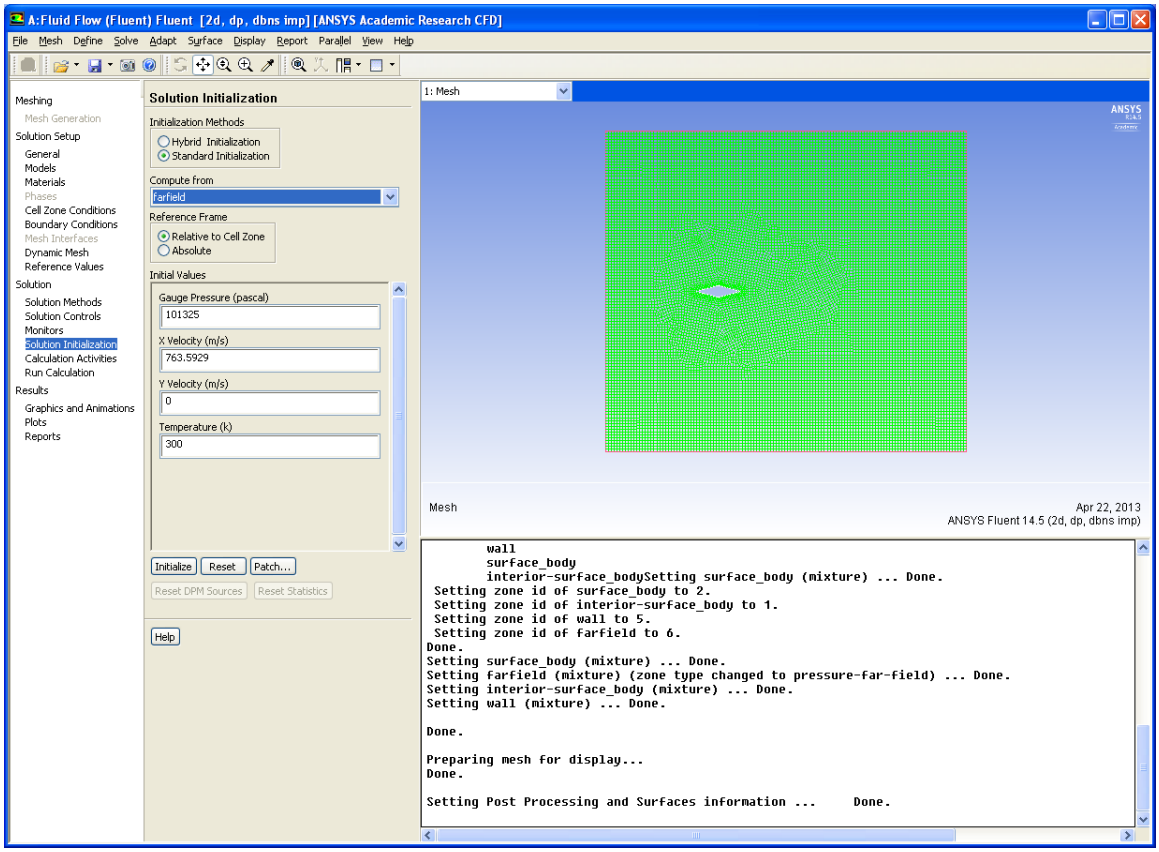

5. Under “Run Calculation,” change the number of iterations to the desired amount (around 5000 to start).

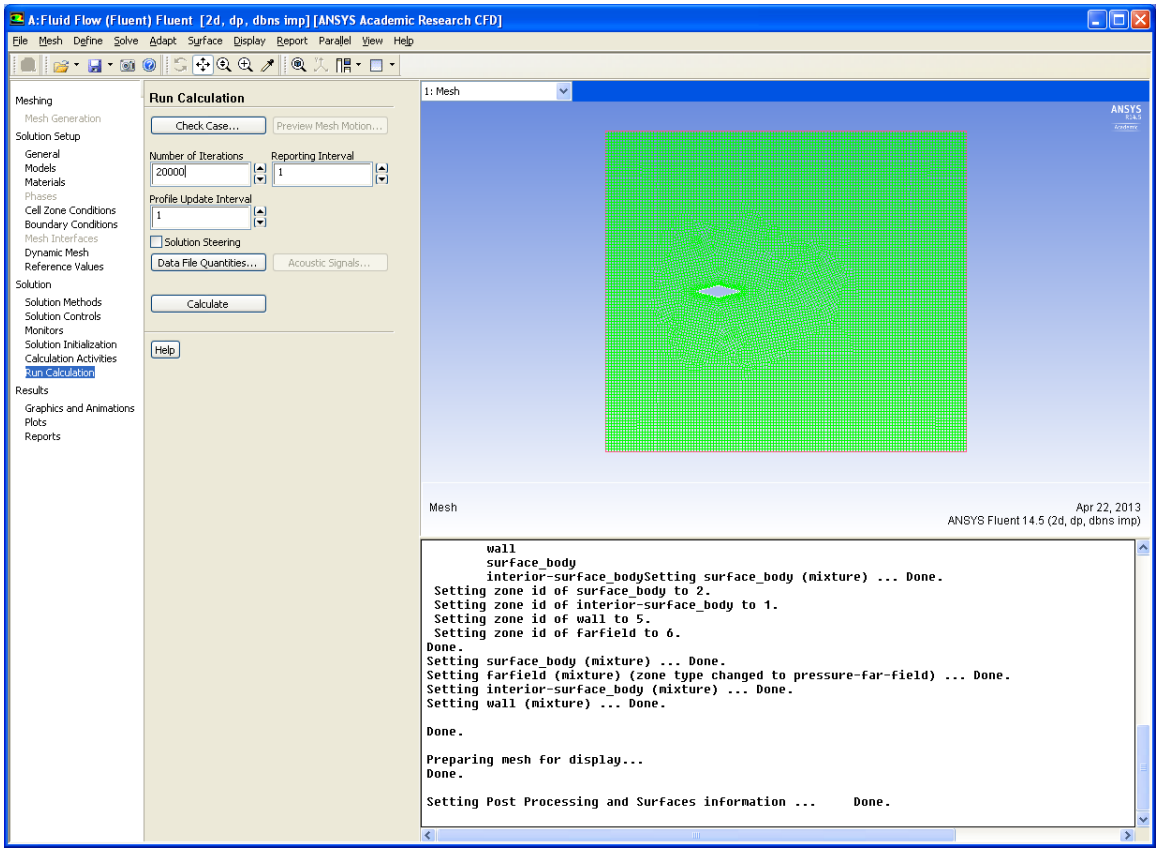

9. Click on “Calculate” to start the solution.

APPENDIX B

Mesh and Solution Data

This table shows the requirements for a good mesh mentioned in the Computational section in the Literature Review. The minimum orthogonal quality ranges from 0 to 1. Values closer to 1 are considered good. The maximum aspect ratio of 5 was met for all cases except Case 10. Case 10 needs to be re-meshed. Only two cases (Case 3 and 4) met the requirement of convergence (<1e-6). Due to time constraints of this project, the cases were not run to full convergence. It is recommended in future work to run the cases the appropriate amount of time.

Case	# Elements	# Iterations	Residuals		Min Orthogonal Quality	Max Aspect Ratio	Fully Converged
			Lowest	Highest			
1	144450	1307	8.78E-03	1.20E-02	0.7559	3.463	
2	174087	18156	6.54E-03	3.60E-02	0.743	3.21	
3	14787	5530	7.34E-07	1.00E-06	0.776	3.52	Yes
4	14753	4180	5.90E-11	9.98E-11	0.786	3.03	Yes
6	91839	1327	1.67E-03	2.78E-03	0.746	2.66	
7	92167	1536	3.24E-03	5.20E-03	0.754	3.595	
8	92607	2159	2.52E-02	4.45E-02	0.758	3.6	
9	92662	411	1.47E-02	6.67E-02	0.701	3.47	
10	102958	1451	6.87E-02	1.64E-01	0.63	5.36	

APPENDIX C

Theta-Beta-Mach Diagram